Manuscript
Click here to view linked References

Modelling the Lava Dome Extruded at Soufriere Hills Volcano, Montserrat, August 2005 - May 2006

Part II: Rockfall Activity and Talus Deformation

A. J. Hale[1]
E. S. Calder[2]
S. C. Loughlin[3]
G. Wadge[4]
G. A. Ryan[5]

1. School of Geosciences, The University of Sydney, NSW 2006, Australia
2. Centre for Geohazards, Dept. Geology, State University of New York at Buffalo, USA
3. British Geological Survey, Edinburgh, EH9 3LA, UK
4. Environmental Systems Science Centre, University of Reading, Reading RG6 6AL, UK
5. Institute of Earth Science and Engineering, University of Auckland, 1142, New Zealand

12th February 2009

Abstract

During many lava dome-forming eruptions, persistent rockfalls and the concurrent development of a substantial talus apron around the foot of the dome are important aspects of the observed activity. An improved understanding of internal dome structure, including the shape and internal boundaries of the talus apron, is critical for determining when a lava dome is poised for a major collapse and how this collapse might ensue. We consider a period of lava dome growth at the Soufrière Hills Volcano, Montserrat, from August 2005 to May 2006, during which a ~100 M m^3 lava dome developed that culminated in a major dome collapse event on 20 May 2006. We use an axi-symmetrical Finite Element Method model to simulate the growth and evolution of the lava dome, including the development of the talus apron. We first test the generic behaviour of this continuum model, which has core lava and carapace/talus components. Our model describes the generation rate of talus, including its spatial and temporal variation, as well as its post-generation deformation, which is important for an improved understanding of the internal configuration and structure of the dome. We then use our model to simulate the 2005 to 2006 Soufriere Hills dome growth using measured dome volumes and extrusion rates to drive the model and generate the evolving configuration of the dome core and carapace/talus domains. The evolution of the model is compared with the observed rockfall seismicity using event counts and seismic energy parameters, which are used here as a measure of rockfall intensity and hence a first-order proxy for volumes. The range of model-derived volume increments of talus aggraded to the talus slope per recorded rockfall event, approximately 3,000 - 13,000 m^3 per rockfall, is high with respect to estimates based on observed events. From this, it is inferred that some of the volumetric growth of the talus apron (perhaps up to 60 - 70%) might have occurred in the form of aseismic deformation of the talus, forced by an internal, laterally spreading core. Talus apron growth by this mechanism has not previously been identified, and this suggests that the core, hosting hot gas-rich lava, could have a greater lateral extent than previously considered.

1. Introduction

Silicic lava domes are often surrounded by an apron of talus derived from rockfall activity. Here we simulate the evolution of one dome growth period at Soufrière Hills Volcano (SHV), Montserrat using an axi-symmetrical Finite Element Method (FEM) computational model for dome growth, comprising of evolving core and carapace/talus components (Hale, 2008). This model grows the lava dome endogenously, by adding lava to the core and adjusting the shape of the talus. Lava dome growth has two end-member styles: endogenous (internal swelling) and exogenous (growth at the free surface). In a companion paper (Hale et al., in review), we discuss the structure of the SHV lava dome and how it varies from dominantly exogenous and dominantly endogenous growth periods. We cannot model purely exogenous lava dome growth using this continuum approach, due to the complexities involved in simulating the extrusion of individual shear-bounded lobes of lava. Hence, by applying our endogenous dome growth model and neglecting exogenous growth processes we make the assumption that we are simulating only the large-scale structure rather than the finer-scale surface physical processes, and that this does not greatly influence the overall growth of the dome. A thorough rationale and justification for this approach is given in Hale et al., (in review). It is clear however, that our model can represent most faithfully, dome growth periods that were characterized predominantly by endogenous growth. We apply this model to a period of continuous dome growth at SHV between August 2005 and May 2006, during which time a ~100 Mm^3 lava dome developed (Jones et al., 2006, Loughlin et al. 2006) and for which the endogenous model is considered reasonable (Hale et al., in review). This dome was the first of two major lava domes extruded during Phase III (August 2005 to April 2007) of the eruption (Ryan et al., in review). Purely endogenous lava dome growth occurred for several short periods between August 2005 and May 2006 and there were significant episodes of shear lobe development believed to have included an endogenous component (Loughlin et al., in review). Thus, volumetrically, endogenous growth was an important contribution to the construction of this particularly large dome. Indeed, this pattern appears to have also been common in the construction of large domes during Phases I and II.

The momentum equations of the dome growth model are formulated in an Eulerian framework and use the parallelised finite element-based PDE solver eScript/Finley (Gross et al., 2007). The free-surfaces of the dome and the core-talus interface are modelled utilising the level-set method,

a technique used to trace flow fronts and boundaries without distorting the model space/mesh (Hale et al., 2007). A shear-thinning viscosity relationship for crystal-rich lava presented by Lavallée et al. (2007) is used and compared with that of lava behaving in a Newtonian manner. In a companion paper (Hale et al., in review) we describe how the internal structure of the modelled dome evolves. Here, we focus on the modelled conversion of carapace to talus, which, on the real dome would correspond to rockfall activity. This activity is observed and recorded via seismic records of individual rockfall events gathered by the Montserrat Volcano Observatory (MVO), and we use these data to test the models.

2. Lava Dome Growth, Rockfalls and Seismicity

Extrusion rates, dome morphology and growth style varied throughout Phase I of the eruption (1995-1998) with average extrusion rates reaching peaks of ~10m^3/s (Watts et al., 2002). During Phase II the extrusion rate was steadier and relatively low, rarely exceeding 4m^3/s (Herd et al. 2005). During Phase III, extrusion rates varied with growth style and dome morphology as in Phase I but average extrusion rates up to 15m^3/s were measured (Loughlin et al., 2006). During periods of low extrusion rate, dome growth was dominated by whalebacks (particularly at the onset of dome growth in 1995) and spines (Watts et al., 2002). During moderate extrusion rates shear lobes dominated and grew for weeks to months; importantly they included both exogenous and endogenous growth. Periods of higher extrusion rates suppressed microlite crystal growth and resulted in the extrusion of lower viscosity lava ('pancake lobes'; Watts et al., 2002).

Dome growth can switch abruptly from entirely endogeneous to dominantly exogenous growth and a well-documented example of this occurred between October and December 1996 (Hale and Wadge, 2008). During this period, a rapidly growing endogenous dome slowed in growth considerably as its height reached approximately 120 m (Watts et al., 2002,). This was followed in mid-November by a directed intrusion into the dome creating a region of uplift over 30 m high. In mid-December growth style changed to dominantly exogenous and a blocky shear lobe was extruded at between 4 and 6 m^3s^{-1}. Then on 25th December 1996 there was a pronounced

pulse of activity, heralded by localised surface doming, and a low-viscosity "pancake" lobe extruded at a rate of 6 to 9 m^3s^{-1} (Watts et al., 2002).

Sequential and frequent collapses of the SHV lava dome occur as a natural consequence of both endogenous and exogenous growth. A continuum of collapse phenomena exists, ranging from lava block rockfalls, through small pyroclastic flows, to major dome-collapse events involving as much as 164 Mm^3 of dome material (Herd et al. 2005). Collapse phenomena can be viewed as a mass wasting process, the rate of which is forced primarily by internal processes such as active intrusion and thrust forces, and gas pressurization. However, external processes such as lava flow front disaggregation as it reaches steep slopes and intense rainfall can also play an important role (Calder et al., 2005, Barclay et al. 2006).

Rockfalls are the small volume end-member of collapse phenomena; they occur frequently, with characteristically between 20-160 rockfalls occurring daily at SHV during periods of active dome growth (Calder et al., 2002). They occur along high-angle failure planes on the outer, largely degassed, carapace of the dome and may involve discrete blocks that roll, bounce or slide downhill, or may be significant avalanches. Rockfalls rarely travel far beyond the base of the talus apron 0.5 - 0.8 km from the dome summit. Rockfall activity is known to correlate with directional and temporal changes in lobe extrusion (Watts et al., 2002), as well as changes in eruption style and extrusion rate (Calder et al., 2002, 2005; Loughlin et al., 2006). Increased rockfall activity also occurs as an immediate result of new batches of magma intruded into the base of the dome and is intimately associated with cyclic crater rim ground deformation (Voight et al., 1999). Calder et al. (2002) characterised two styles of rockfall generation, active and passive. Actively generated rockfalls are those sourced from actively growing areas on the dome surface and involve the disintegration of hot material newly extruded at the dome surface. While passively generated rockfalls, occur as isolated events anywhere on the dome surface involving largely degassed, cooler carapace material. These distinctions were made on the basis of a) previous identification of the active growth regions, and b) observed differences in the vigour of convection in the associated ash clouds from the relatively hot or cool source materials respectively.

Pyroclastic flows are distinguished from rockfalls by their larger size, longer run-out distances (>0.5 km), and greater component of fine material, resulting in appreciable buoyant ash clouds. Deposit volumes are typically in the order of 10^4-10^6 m^3 for small to medium-sized (1-3 km run out) pyroclastic flows (Calder et al., 1999; Cole et al., 2002). Large dome collapses, in excess of 1 x 10^6 m^3, have occurred on 47 occasions throughout the eruption to date (Calder and Bernstein, 2007). These collapses commonly occur as retrogressive failures of the dome over an extended period of time (minutes to hours) and excavate spoon-shaped cavities to depths of 400 m.

Both rockfalls and pyroclastic flows at the SHV excite distinctive emergent high frequency seismic signals on the MVO seismic network, as the dense, block-rich, material impacts the ground surface as the flow propagates downslope (Luckett et al., 2002, Calder et al., 2002). Relatively little work has been carried out on the seismic signals of rockfalls and pyroclastic flows from any lava dome eruption (Zobin, 2003). Their analysis is particularly complex due to their source mechanisms involving, a) a transfer of an unknown mass of material at the surface and, b) a source footprint which changes size, shape and location with time. For example, the duration of the signal produced by these avalanches corresponds to the time the avalanche spends travelling over the ground surface (a function of distance covered and flow velocity) as well as, and importantly, the dispersion effects of the seismic signal which are not well constrained. Seismic amplitude is determined by a combination of factors, including rockfall mass, height of dome (potential energy), slope angle, and the damping behaviour of the unconsolidated substrate that can change with time. Furthermore variations in amplitude can occur as a result of the pulse-like nature of flow generation, due to retrogressive collapse initiation (Loughlin et al, 2002), but also as a result of the pyroclastic flows changing proximity to the geophones as they approach and subsequently pass-by the stations (Jolly et al., 2002). Some pyroclastic flows, and most rockfalls, are only observed seismically and thus the seismic data, irrespective of its complexities, provides one of the most important and complete records for the collapse history of the dome.

Rockfall seismicity parameters, such as event duration, maximum amplitude, energy, frequency content, and repose period are extracted from the continuous seismic data records by task-specific algorithms. In order to compare with the model results, we use both the number of

rockfall events per day (referred to as event counts) and the measure of total energy (J/Kg) as first-order indicators of the relative volume of material being shed as rockfalls with time. Both these parameters provide a somewhat imperfect account of the accumulating talus volume. For example, rockfall seismic event counts neglect variations in event magnitude, and a reasonable estimate is that individual event magnitudes could range over 4 orders of magnitude ($10^1 – 10^4$ m^3), meaning that event counts only provide a time-averaged accumulation rate over the duration of the dome-forming period. Rockfall energy or, strictly speaking energy density (J/Kg), is calculated by the SEISAN program as the sum of the squared amplitudes (measured in ms^{-1}) of the seismic record. This value is the number closest to a total source energy measurement that can obtained for rockfall or pyroclastic flow waveforms, since conventional techniques to calculate source energy for standard earthquakes cannot be applied to this type of rockfall seismic signal. Energy density measurements are complicated by time-varying path effects (such as the development of a thick talus substrate and changes in the impact of the rockfalls with the crater wall), and vary from station-to-station depending on local path effects as well as proximity to a particular rockfall changing during run-out. A thorough analysis of the rockfall seismic data is required, but is beyond the scope of this paper. Here, and in the absence of better parameters, we use the event counts and the variation in energy density as first-order proxies for the rockfall accumulation with time. Previous work illustrating clear relationships between the rockfall seismic data and the nature of observed dome growth and instability (Calder, 2002; Calder et al., 2005), suggests this approach is valid.

3. Computational Model, Lava Properties and Model Set-Up

Conceptually we can divide the lava dome into three units; a relatively intact and ductile interior (the core), a largely degassed region of intact lava that remains attached to the outer surface of the core (the carapace), and a granular, friction-controlled more distal region (the talus). The disaggregating carapace provides the source of the talus once it becomes critically unstable. Following Hale (2008) we do not explicitly model the carapace and talus as separate domains, but rather the same region representing solidified degassed lava (Fig. 1). In our model, dome growth occurs at two timescales: continuous dome expansion, via the addition of new lava into the ductile core interior and relatively instantaneous conversion and readjustment of part of the

carapace to talus once it oversteepens, as will be discussed in more detail below. The model boundaries, a typical mesh and key terms used in this paper are illustrated in Fig. 1.

Although the rheology of crystal-rich lava is reasonably well understood (Lavallée et al., 2007), the rheology of the talus is not well-constrained, and in reality is likely to vary spatially, with burial. For simplicity, we model the deformation of the entire dome (including the talus) as a ductile fluid. Silicic lava has a low Deborah number (a measure of how fluid a material is given the time-scales modelled or observed) and we assume the same for the talus components, but allow the viscosity to vary between the core and carapace/talus regions. The incremental process of the conversion of carapace to talus and carapace/talus readjustment is treated as a frictional-controlled granular material with a defined angle of repose.

A solidus pressure isobar is used to determine where core material turns into carapace/talus, a one-way process in this model. This condition is used for two reasons. First, it is well known that as magma ascends and the pressure decreases, volatiles can be exsolved promoting crystallisation and solidification (Cashman and Blundy, 2002; Hort, 1998). Intermediate lava, such as the andesitic lava of Soufrière Hills Volcano, is dominated by degassing-induced crystallisation with cooling being negligible during lava dome emplacement (Sparks et al., 2000). Therefore the solidus pressure can be used to mark the transition to a solid state (Simmons et al. 2005), and we simplify our model by assuming that only degassing-induced crystallisation contributes to the growth of solid lava, i.e. the carapace/talus, and neglect cooling. The second reason is that a transition to a solid state as described by the solidus pressure is relatively easy to implement computationally (Hale, 2008).

3.1 Model Formulation

During a single time-step of the model, we first calculate the velocity and pressure fields of the dome material, talus and core, and grow the dome accordingly. Next, the extent of the carapace/talus interface within the dome is re-calculated and the interface updated. The interface between the carapace/talus and lava core is identified using knowledge of the existing core region. The updated core region corresponds to where the dome has a pressure greater than or equal to the solidus pressure and where the dome material was originally designated as core. The

updated carapace/talus region corresponds to regions where the core has a pressure less than the solidus pressure or where dome material was originally designated as carapace/talus. This prevents talus from being converted back into core material if the pressure becomes greater than the solidus pressure, which does not happen in reality, hence the necessity for tracking this interface. Lastly, the clastic nature of the talus allows readjustments so that it becomes gravitationally stable. Hence, clastic material is displaced to rest at the angle of repose, which entails the final stage during a model time-step. These sub-steps are repeated continuously to allow the lava dome to grow in time. See Hale (2008) for a thorough discussion of this model. The axi-symmetric lava dome grows onto a horizontal base fed by lava from the conduit exit applied as a parabolic velocity field.

3.2 Lava Properties and Model Set-Up

Our model requires several input parameters including: the viscosity of the lava in the core and talus regions, the extrusion rate or driving pressure, the solidus pressure, the friction angle for the talus, and the shape of the lava dome base (Hale, 2008). We have parameterised the model with values appropriate for the August 2005 – May 2006 growth period on SHV, but the model is generic and can be applied to other volcanic systems. Dome growth is assumed to have begun at 00:00hr on 1st August 2005. Our simulation starts with a small mound of lava above the conduit vent corresponding to dome growth at a time of 0.45 days, a simulation start time of 10:48hr on 1st August 2005, and has a volume of 10,150 cubic metres (0.01% of the final dome volume). The lava dome collapsed on 20th May 2006, 292 days after extrusion began and this corresponds to the end of the simulation. Dome growth is assumed to be axi-symmetric in a model space 450 m high and 500m in the radial dimension. A first-order element type is used with an element spacing of 2.5 metres. We now discuss appropriate values for these parameters and summarise them in Tables 2 and 3.

3.2.1 Viscosity

The lava extruded at SHV contains abundant crystals and bubbles with a crystallinity estimated to be between 65% and 95% (Sparks et al., 2000). Lavallée et al. (2007) performed viscosity measurements on crystal-rich lava, resulting in a singular dependence of viscosity on the strain-rate regardless of the geochemistry, the crystal content, and up to 25% bubbles. We use the

shear-thinning viscosity relationship without yield strength as presented in Lavallée et al. (2007) for crystal-rich lava (Eqn. 1),

$$\log \eta_b = -0.993 + 8974/T - 0.543 \log \dot{\gamma}. \quad (1)$$

Where η_b is the effective viscosity in Pa s, T is the temperature in degrees centigrade (a constant value of 830ºC is used here (Barclay et al., 1998)), and $\dot{\gamma}$ is the strain-rate. One limitation with this relationship is that as the strain rate goes to zero, the effective viscosity goes to infinity. Therefore, a minimum strain rate cut-off value of 10^{-5} s^{-1} is used. This corresponds to a maximum viscosity of 3.4×10^{12} Pa s. This is reasonable because Caricchi et al. (2007) showed that lava samples behave in a Newtonian manner for strain rates below 10^{-5} s^{-1}.

3.2.2 Geometry

The approximate height of the vent for SHV lava dome on 1st August 2005 was at 680 m above sea level (a.s.l.) (Loughlin et al., 2006) and the dome base is assumed to be a flat horizontal plane for our simulations. In reality, the August 2005 – May 2006 SHV lava dome grew within a relatively open crater, with a base which sloped at approximately 12 - 15º to the ENE (Hale et al., in review). For simplicity, we assume that the dome was extruded approximately axi-symmetrically, allowing us to model the dome using axi-symmetrical coordinates to significantly reduce the computer solving time. Until the lava dome is sufficiently large that its growth starts to be influenced by the crater wall, axi-symmetrical growth is considered a reasonable approximation.

3.2.3 Volume

The lava dome grew within English's Crater, which is open to the east-northeast. This means that pyroclastic flows and talus were constrained by the crater walls in all other directions until the summit of the dome reached a height greater than approximately 960 metres above sea level (Wadge, in press). Between 3% and 12% by mass of the dome was converted to pyroclastic flow deposits during August 2005 – May 2006, however we make no explicit account for this in the model. Mass-loss due to energetic pyroclastic flows may be an important process at later times in the growth of the dome and could be easily implemented into the dome model by adjusting the

dome free-surface. However, without detailed observations of this process it would be inappropriate to introduce this variable into the model at this stage.

3.2.4 Density

In the natural system, the process of talus formation can act to increase the volume of talus with respect to the more compact carapace from which it is sourced. This volume change results in a density change; however, for simplicity we neglect any density change from core to carapace to talus in our simulation. Furthermore, the rheological properties of the lava dome may vary substantially within the dome. As the talus wedge gets thicker the more basal parts may increase in density and become stronger by pressure-induced tighter packing of clasts.

3.2.5 Extrusion Rate

Using the MVO survey data of the dome volume for the period August 2005 to May 2006 (Loughlin et al. 2006; Ryan et al in prep), the volume change with time can be calculated. The process of talus formation increases the volume of talus compared to compact carapace or core. Wadge et al. (2008) used a ratio of 0.86:0.54 for core to talus to normalise the resultant volumes, but because we cannot account for separate core-talus volumes throughout this period we do not apply this here. In Figure 2 a best fit curve for the change in volume of the dome over time is applied and the cumulative volume V (M m^3) is approximated as:

$$V = 3.73\times10^{-6} t_d^3 + 2.76\times10^{-5} t_d^2 + 2.20\times10^{-2} t_d, \qquad (2)$$

where t_d is the time in days. Using this best-fit volume-time relationship, the extrusion rate is obtained by taking the gradient, and this is what we use as the input for the model.

3.2.5 Talus Friction Angle

The angle of repose for the lava dome talus can vary spatially from being relatively steep (43 - 32^o) near the carapace-covered core (Fig. 4 in Hale et al., in review), to less steep (<32^o) more distally. These values are consistent with talus slope of 30-43.5^o degrees measured by AVTIS during 2006 (Wadge et al., 2008). Our model has a fixed value for the talus angle of repose through the duration of the simulation, but we vary it's magnitude between 37º and 43.5º in

different simulations. Conventionally, it is assumed that the slope of the talus is considerably lower, approximately 33º, however, this appears not to have been the case at least during the periods measured. During the course of the eruption, the talus angle of repose on different flanks of the dome has been observed to vary, and this variation is probably a reflection of how the talus was deposited. For example, during periods of primarily exogenous dome growth, there are often numerous energetic rockfalls or pyroclastic flows and the resulting talus slope is lower than its critical angle of repose due to the additional kinetic energy associated with these flows (Lube et al., 2005). However, during periods when dome growth is predominantly endogenous or where there are fewer energetic rockfalls or pyroclastic flows, the resultant talus slope rests closer to its critical angle of repose.

3.2.6 Solidus Pressure

The solidus temperature is not well constrained at low pressures, but during the growth of the lava dome on SHV in early October 1996, Watts et al. (2002) noted that the rubbly carapace was only a few metres thick. This suggests that the solidus pressure can be relatively small. A carapace with a thickness of 10 metres is equivalent to a solidus pressure of approximately 0.34 MPa when considering gravity and atmospheric pressure alone. A range of values from 0.2 to 0.6 MPa are used (Table 3).

4. Results

We present the result of eight simulations, seven using a shear-thinning viscosity relationship (Lavallée et al., 2007), and one using a Newtonian viscosity relationship (Table 3). The solidus pressure and friction angle are the parameters varied in the simulations because all the other main parameters are relatively well constrained. When using the strain-rate dependent viscosity relationship (Eqn. 1) we apply a strain-rate cut-off value of 10^{-5} s^{-1} for the core/talus corresponding to maximum viscosity of 3.4×10^{12} Pa s, so that viscosity does not tend to infinity (as described in Hale et al., In review). We acknowledge that it may not be appropriate to model the talus as having the same viscosity relationship as the core. In the talus, fine-grained infill and incipient cementation may start to develop a cohesive strength. The reduction of porosity by rotation, grain deformation and fine grain infill will increase grain contact surface area and hence

bulk friction coefficients. Thus the internal friction of the talus may increase and to account for this change in bulk system properties we can increase the strength of the talus with respect to the core properties. Therefore, we also simulate dome growth using a shear thinning, strain-rate dependent, viscosity relationship (Eqn. 3) with a strain-rate cut-off value of 10^{-5} corresponding to maximum viscosity of $3.4x10^{12}$ for the lava core, while the talus has a viscosity ten to thirty times higher than the maximum cut-off viscosity used for the core. The range of values for the models is given in Table 1, while the specific values for simulations are given in Table 2.

We first consider a generic model of lava dome growth and talus generation for fixed extrusion rates to observe the extent of talus development. Following this, we consider lava dome growth at SHV for one particular period of dome growth from August 2005 to May 2006 using the observed volume and hence time-dependent extrusion rate (Fig. 2).

4.1 Generic Dome Growth Models

Our generic dome model uses both a shear-thinning viscosity relationship (Lavallée et al., 2007) and a constant Newtonian viscosity of $3.4x10^{12}$ Pa s. We use a talus angle of repose of 40º, an appropriate intermediate value for the observed slope of the talus on Soufrière Hills Volcano (Wadge et al., 2008), a conduit radius of 15 metres, a lava density of 2350 kgm^{-3}, and a solidus pressure of 0.4 MPa, including atmospheric pressure, to model dome growth for four constant extrusion rates (2, 4, 6, and 8 m^3/s). These simulations provide a generic understanding of how the talus grows and re-adjusts in the models, as well as how extrusion rate variations influence the rate of talus growth.

4.1.1: Height and Radius of the Lava Dome

The growth of the dome is essentially self-similar, i.e. exhibiting the same maximum height and radius, for a given dome volume. However, as shown, the volume of talus adjusted and core volume fraction can vary significantly depending upon the extrusion rate (Fig.3).

4.1.2: Talus Adjustment Location

The first stage of each simulation iteration involves the injection of fresh lava into the dome core, often resulting in the free-surface of the dome resting at angles greater than the angle of repose. In stage two we adjust the free-surface of the lava dome so that it rests at angles equal to, or lower than, the talus angle of repose. We do this by evaluating the free-surface angle over the entire dome surface using the level-set field (Hale et al., 2007). Using this information we can calculate a radius, R_a, the minimum distance from the centre of the dome, beyond where the free-surface angle exceeds the talus angle of repose, as shown schematically in Figure 4a. Therefore, R_a is an indication of where the dome was uplifted during the fresh lava injection stage to angles beyond the talus angle of repose. From R_a to the maximum lateral extent of the dome also indicates where talus is primarily adjusted on the dome surface.

The ratio, R_a/R, (where R is the maximum lateral extent of the talus) is shown in Figure 5 for the generic simulations. When $R_a/R \approx 0$, R_a is very small relative to the maximum radial extent of the dome and the over-steepened area is very close to the summit. Talus adjustments occur over the remaining extent of the talus slope, meaning that the dome shape is approximately conical. However, when $R_a/R \approx 1$, R_a is large relative to R, and talus adjustments only occur at the outer extent of the talus slope, meaning that the dome shape will tend to a truncated cone with a convex top as shown schematically in Figure 5c. From Figure 5 the ratio R_a/R changes most when the dome is small, and as the dome grows larger it stabilises.

Both model results using a Newtonian and shear thinning viscosity relationship for dome growth have low R_a/R ratios, between approximately 0 and 0.2, suggesting a near-conical shape. There appears to be little difference between the R_a/R ratios for the different simulated extrusion rates except at later times and only for the dome growth model with the lowest extrusion rate. For the 2 m^3s^{-1} extrusion rate, R_a/R increases as the dome volume increases beyond 20 M m^3, suggesting that the dome is departing from being nearly conical to having a flatter, wider top (Fig. 5c). This

is due to greater lateral spreading of the core due to gravity, which is more pronounced for lower extrusion rates, forcing R_a to larger radial values. All these results suggest that most of the talus adjustments occur over a very large region of the dome surface from close to the summit of the dome to the maximum lateral extent of the dome. This is consistent with observations of rockfalls at SHV, which are largely sourced from the upper, blocky regions of the dome close to or at the summit (Calder et al., 2002).

There are several effects that contribute to the scatter in these results. First, to calculate the angle of the dome free-surface we must consider a region one element wide that surrounds the zero isoline for the level-set which describes the dome free-surface, to ensure that there are elements within this region that are close to the dome surface (Hale et al., 2007). Second, the finite spacing of the mesh means that when the free-surface angle is calculated, the angle is only calculated at nodes on the mesh. This corresponds to only knowing the free-surface angle every 2.5 metres radially (an interval approximately equal to 0.5% of the total domain). Reducing the element size reduces the degree of scatter, although at the expense of increasing computational solving time without changing the overall model results.

4.1.3: Talus Readjustments

Our model also records the volume of carapace/talus readjusted per second. This volume corresponds to the volume of the model domain occupied by carapace or talus before the angle of repose readjustment sub-step, minus the volume of the domain occupied by carapace or talus directly following the readjustment sub-step and divided by the time-step duration (Fig. 4a). The best way to conceptualize this volume is that it is analogous to the volumetric additions, or aggradation of, talus material on the dome flanks by rockfalls (Fig. 4b). That is, during the growth of the dome, material is forced to angles above its angle of repose, then during the talus adjustment sub-step (the equivalent of rockfall activity) this volume is redistributed along the flanks of the dome at its angle of repose. Fresh talus material is sourced from the carapace at the dome summit, from $0 < R < R_a$, while readjustment of existing talus material occurs between R_a and R. Talus readjustment rates through the history of the generic dome growth are shown in Figure 6. The talus readjustment rate scales with the extrusion rate and is approximately

constant, with minor fluctuations (~1 m^3/s). It should be noted that the talus volume readjusted can be larger than the input volume because the talus readjusted volume can include existing talus in addition to fresh carapace.

4.1.4: Carapace Generated

Our model saves information for the volume of carapace generated per second. This corresponds to the volume of the domain that changes from core into carapace/talus after being displaced into regions of the dome that fall below the solidus pressure during each time step, divided by the length of the time-step (Fig. 7). The carapace production rate generally decreases with time (Fig. 8). Scatter in this result is due, in part, to the way in which R_a is calculated, given the finite element spacing as described in section 4.1.2, which affects the location of the carapace-core interface. Also, since the volume is calculated by interpolating the axi-symmetrical area and integrating by 2π this process leads to some degree of rounding error. Lastly, when the dome is small there are relatively more carapace and talus adjustments because the dome radius is growing more quickly (Fig. 4 a,b).

The rate of generation of carapace approximately scales with the extrusion rate both for a Newtonian and shear-thinning viscosity relationship (Fig. 8). Early in the simulation the rate at which carapace is generated is very close to, or higher than, the rate at which lava is extruded, but over time this value decreases. This is because early on, carapace is generated across the whole surface of the dome, the surface of which is initially changing rapidly, while later it is primarily generated over the summit region as the dome core becomes flanked by a wide apron of talus (Hale, 2008).

4.1.5: Average Carapace Generated and Talus Readjusted

The average rates of carapace generated and talus readjusted for the four different extrusion rates modelled over the entire simulation (a final dome volume of 30 million cubic metres) are shown in Figure 9. The relationship between both the average carapace generation rate and the talus adjusted rate, and the extrusion rate is linear. This relationship is corroborated by various observations that rockfall activity, to a first order, varies with extrusion rate (Calder et al., 2005)

and that at a larger scale pyroclastic flow is also extrusion rate dependant (Yamamoto et al., 1993; Uhira et al., 1994).

For both Newtonian and shear-thinning viscosity models, the rate of carapace generation is less than the rate of talus readjustment. This is because the rate at which carapace is generated only includes material that converts from core into carapace. While, the rate at which talus is readjusted includes adjustments from pre-existing talus as well as carapace. Further, as the lava dome grows, new carapace is confined to the central summit region because the talus layer surrounding the core becomes thicker further from the dome. However, carapace/talus adjustments can occur all over the dome surface. For the Newtonian lava dome model, the time-averaged proportion of extruded lava converted to carapace compared to the extrusion rate is between 80 and 83%, while for the shear-thinning viscosity lava dome model the rate is 68 to 70% (Table 1). This suggests that the Newtonian lava dome model experiences a larger amount of carapace removal from near the summit of the dome, permitting new carapace to form, than for the shear-thinning viscosity model. Another way to view these results is that these simulations suggest that approximately 70 to 83% of the core lava is channelled to the free-surface of the dome to be converted into carapace in what could be considered a largely exogenous manner. Because the shear-thinning viscosity model can be expected to favour greater lateral spread than the Newtonian viscosity model (i.e. a viscosity drop near the conduit exit where shear stresses are highest), less lava is channelled vertically and subsequently converted into carapace. Hence the lava dome model with a shear-thinning viscosity relationship behaves more endogenously than for the Newtonian lava dome.

For the Newtonian lava dome model, the average rate of talus readjustment is between 98 and 112%, of the extrusion rate, while for the shear-thinning viscosity lava dome model it is between 93 and 99%, for the extrusion rates considered (Table 1). This difference between the viscosity relationships means that larger talus readjustments are required for the Newtonian viscosity relationship models and the talus can be considered more mobile. Since, shear-thinning permits greater lateral spread of the core by creating a viscosity drop near the conduit exit, this results in freshly extruded lava preferentially spreading laterally as opposed to forcing larger regions of the dome surface to angles beyond its angle of repose.

As observed previously, the rate of carapace volume generated, as well as the rate of talus volume readjustment changes as the dome volume increases (Figures 6 and 8). Therefore, calculating the average volume of carapace generated or talus readjusted per second for the entire simulation is an over-simplification of the processes. Although not explicitly shown here, it might be expected that when the dome is small a larger volume of carapace is generated (evidenced by increased carapace generation rates) and therefore the lines in Figure 9 would shift upwards (as the rates increase for all extrusion rates), while at later times in the growth of the dome less carapace is generated and the line in Figure 9 would shift downwards (as the rates decrease for all extrusion rates). This will also be true for the linear relationship between the extrusion rate and talus volume readjustment.

4.1.6: Core Volume Fraction

For each time-step the model records the total dome volume, as well as the volume of the dome occupied by core and carapace/talus components for our generic simulations. The total core volume fraction initially increases rapidly, from ~ 0.15 to 0.2 for the Newtonian model, and from ~0.15 to 0.3 for the shear-thinning viscosity model (Figure 10a,b) and then continues to rise slowly. However, the largest increase in core volume fraction within the lava dome occurs for simulations with the lowest extrusion rate; the final core volume fraction varies between 0.23 and 0.43 for the Newtonian model, and 0.39 and 0.55 for the shear-thinning viscosity model, for the simulated extrusion rates of 8 m^3s^{-1} and 2 m^3s^{-1}, respectively.

Profiles of the dome surfaces and core-talus interfaces for two, 11.5 million cubic metre volume, domes extruded at rates of 2 m^3s^{-1} and 8 m^3s^{-1}, using the shear-thinning viscosity model are shown in Fig. 10c. The high extrusion rate (8 m^3s^{-1}) profile shows less lateral spreading for the core (black line), than that for a low extrusion rate (2 m^3s^{-1}), in which a higher degree of lateral spread of the core is evident (grey line). Observe that the total dome volumes and shape (constrained by free-surface adjustments) are the same, however the low extrusion rate dome develops a larger core and hence a larger volume fraction of core for the same total dome volume. Also, note that in the simulation with the highest extrusion rate, lava is channelled primarily vertically towards the free surface, where it can readily be turned into carapace and

distributed down the flanks of the dome as talus. This can also be conceptualized as forcing the model towards behaviour which would be manifest as large-scale exogenous growth. However, in reality lava is channelled to the free surface during exogenous dome growth along internal discontinuities known as shear bands (Hale and Wadge, 2008). Lava dome surfaces and core-talus interfaces for the two viscosity models can also be compared (Figure 10d). Again, for an 11.5 million cubic metre dome volume, extruded at 8 m^3s^{-1}, the shear-thinning viscosity model (grey line) experiences significantly more lateral spread of the core than for the Newtonian viscosity model (black line). Shear thinning occurs near the conduit exit within the dome, creating a region of lower viscosity and enhancing lateral spreading. These data also explain the observed differences in core volume fraction generated by the two viscosity models (Figure 10a,b), where the shear-thinning model generates the largest core.

4.2. Soufrière Hills Volcano Lava Dome: August 2005 to May 2006

We now consider a 292-day period of almost continuous dome extrusion at the Soufrière Hills Volcano (SHV), which comprises one complete dome growth cycle from its initial extrusion within an empty crater on 1 August 2005 until its destruction on 20 May 2006. Survey observations of dome volume (Fig. 2) are used to drive the model growth rate and the model results are then compared to the record of rockfall seismic activity. We present results for eight simulations using both shear-thinning and Newtonian viscosity models. The parameter ranges for the models are given in Table 2, while specific simulation values are given in Table 3. A thorough discussion on the internal structure of the dome, i.e. the location of the core and talus within the dome for these parameter values are discussed in more detail in the companion paper (Hale et al, in review).

4.2.1 Carapace Generated

The rate of carapace generated is calculated by our model as described in Section 4.1.4 and shown in Figure 11a. Except for Simulations 6 and 7, which use a higher viscosity for the talus region, the rate of carapace generation shows some time dependence. The time-dependency of this relationship is due to two competing effects: 1) the volume of lava converted into carapace increases because the rate of lava extrusion increases, and 2) the volume of core converted into

carapace decreases at later times because the dome becomes enshrouded with carapace/talus most predominantly laterally from the dome core, and therefore the core-carapace interface moves away from the free-surface, except near the dome summit. The ratio of carapace generated to extrusion rate is a measure of the relative rate of development of the carapace (Figure 11b), and also shows time dependency through the dome growth history. These results are consistent with those observed in Section 4.1.5, such that the volume of carapace generated with time is initially approximately proportional to the extrusion rate, i.e. the percentage of intruding mass converted into carapace is initially close to 100%.

For simulations with a uniform viscosity relationship (Newtonian or shear-thinning) for the core and talus (simulations 1 to 5 and 8), the rate of carapace generation increases to a peak of approximately 3 m^3s^{-1} (Fig. 11a). After about 150 to 200 days, the carapace generation rate decreases (Fig. 2). The timing of the peak appears to depend upon the modelled angle of repose for the talus. For Simulations 1 to 3 and 8, which have an angle of repose of 43.5º, the peak falls between days 160 to 175 (late-January to early February 2006), while for Simulation 4 (with an angle of repose of 40º), the peak is close to day 190 (late-February 2006), and for Simulation 5 (with an angle of repose of 37º) there is a broad peak maximum close to day 210 (mid-March s2006). Following this peak, the volume of carapace generated then decreases, and this is most prominent for simulations with higher angles of repose for the talus. Simulations 6 and 7, in which the talus has a frictional "strength" show rates of carapace generation rising throughout, up to about 6 m^3s^{-1}, which suggests that lava is preferentially channelled vertically due to the surrounding strength of the talus.

The amount of core volume converted into carapace per time-step is initially very high (Figure 11b), approximately 100%, decreasing later to 10 to 50%. The volume of carapace generated can be greater than the volume of lava extruded during each time step due to talus adjustments exposing a larger volume of core than just the newly extruded volume. This suggests that the volume of lava added to the core pushes a progressively smaller amount of core into regions below the solidus pressure as dome volume increases (Figure 11b, c). The model suggests that dome growth should behave more endogenously with time (i.e. a smaller proportion of lava core is converted into carapace). Simulations 6 and 7 show slightly different behaviour, with a core to

carapace conversion percentage from 90% falling to 60%. This can be viewed as dome growth becoming primarily endogenous, i.e., less core is converted into carapace and core must be spreading laterally within the dome. However, this can still result in talus readjustments (Fig. 11c), due to the spreading core slowly deforming the free-surface beyond the talus angle of repose prompting readjustments of the talus.

4.2.2 Talus Readjustments

Results for the August 2005 – May 2006 dome simulations show that the rates of talus readjustment (Figure 12a) increase as the dome grows and the extrusion rate increases. This is consistent with results in Section 4.1.4. A relatively constant relationship is found when the volume of talus readjusted per second divided by the extrusion rate (equivalent to the volume fraction of talus material readjusted relative to the intruded mass) is plotted against time (Figure 12b). The result of unity, with some degree of scatter, implies that the proportions of extruded material and deformed talus by readjustment remain approximately constant throughout the dome growth simulation.

The difference between the rate of carapace generated with respect to extrusion rate and the rate of talus readjustment with respect to extrusion rate reflects that early on in the growth of the lava dome, the carapace generated rate is approximately the same as the talus deformation rate. While at later times the dome becomes flat-topped and the core-talus interface moves away from the free surface of the dome at the lateral extent of the dome, permitting core to be converted into talus only in the central summit region (Hale et al., in review). Later in the evolution of the dome therefore, the ratio of talus readjustment to carapace generated increases considerably. This can be viewed as the core volume with respect to the total dome volume increasing with time as shown in Hale et al. (in review).

4.2.3 Comparison to Rockfall Seismicity Data

A taxonomic view of the relationship of clastic rock generation and movement to lava dome growth at Soufrière Hills Volcano is shown schematically in Fig.13. The primary division is

between rockfalls generated actively and passively (Calder et al., 2002). The active branch is dominated by events that are recorded seismically. The passive branch, on the other hand, comprises mainly smaller magnitude events many of which could be potentially aseismic. Some of these can be envisioned as events that are caused by local perturbations of the talus which just exceeds the stability threshold while others will be forced internally by endogenous growth. The relationships between the volume of material involved in a rockfall event and the frequency of occurrence and energy released are almost certainly non-linear. In Figure 13, we show schematically that the two relationships between volume and frequency and energy that are used to compare with the model results will themselves depend on the boundaries chosen between seismic or aseismic rockfall events and pyroclastic flow events at either end of the collapse spectrum. The inflection shown at the rockfall – pyroclastic flow boundary indicates the change in mechanical behaviour as the fluidised pyroclastic flow regime develops.

Figure 14 shows the cumulative number of rockfalls recorded, used as a proxy for the volume of talus material deposited or adjusted, during the August 2005 to May 2006 dome growth period. The curves of simulated cumulative talus readjusted with time are similar to that measured from seismic data derived from rockfall activity (Fig.14a) with some notable differences. Figure 14b shows the equivalent cumulative volume of carapace generated during the dome growth period using our simulation, which also represents the total volume of talus within the dome. We plot this because the cumulative number of rockfalls multiplied by an assumed volume per rockfall can be used as a first approximation to estimate the total volume of talus within the dome. However, it is not appropriate to assume that all rockfall seismic signals are sourced from active rockfalls generated by unstable carapace. For our simulations the volume of carapace generated represents a minimum for the volume of talus material adjusting at the dome surface. The cumulative volume of talus material readjusted corresponds to the maximum volume of material that is adjusted at the dome surface, including the deformation of new talus (carapace) and the readjustment of pre-existing talus. Compared to the total talus volume within the dome (Fig. 14b) the cumulative volume of carapace/talus adjusted (Fig. 14a) can be approximately double.

Simulation 3 used the highest solidus pressure modelled and results show that a larger volume of talus is readjusted (Fig. 14) and that the total volume of carapace generated is higher, compared

to Simulations 1 and 2 that have a smaller solidus pressure but where all other parameters are held constant. Simulations with a smaller angle of repose (i.e. Simulations 4 and 5) result in a larger amount of talus being generated (Fig. 14b) compared to Simulation 2, which has the highest talus angle of repose. This is because domes with a lower angle of repose require a larger talus volume (i.e. the lateral extent of the dome will extend further) relative to a dome with a higher angle of repose. Our simulation using a Newtonian viscosity model (i.e. Simulation 8) produces a higher volume fraction of talus when compared to the purely shear-thinning viscosity models, consistent with results in Section 4.1.6. There is less lateral spread of the core due to a reduced viscosity near the conduit exit where shear stresses will be highest. Simulations 6 and 7 that have a higher viscosity in the talus region, produce the largest amount of carapace as well as talus readjustment. This is because the higher viscosity in the talus region confines lateral spread and forces the extruded lava to be channelled primarily vertically, with the talus essentially acting as a buttress.

The plateau in rockfall seismicity between days 160 and 200 included two periods of high extrusion rate that resulted in the emplacement of 'pancake lobes' (Loughlin et al., 2006; in review). These lobes generated very few rockfalls and may have included an endogenous component. The rapid change in the seismic data-set at approximately day 200 represents a significant change in dome growth style and direction, from a rather localized northerly-directed shear lobe to a significant shear lobe directed towards the ENE. Extrusion in this direction (towards the open, downslope side of the crater), always resulted in more frequent and widespread rockfalls than extrusion in other directions. Likewise, the peak at approximately day 260 corresponds to development of a ENE-directed shear lobe, and a plateau at ~280 days represents a period when extrusion rates remained high but there was little obvious surface expression or rockfall activity. This was probably an episode of mainly endogenous dome growth. The final peak at approximately day 285 represents the extrusion of a megaspine, followed by endogenous growth (Loughlin et al., in review).

4.2.4 Rockfall Seismicity Data Complications

It should be stressed that the seismic data-set as-is, cannot be expected to provide a complete nor accurate history of talus accumulation on the lava dome. The seismic network does not for

example, record very small volume/duration rockfall events that generate signals which are either below an energy threshold or shorter than ~2 seconds in duration. Thus, as the dome grows larger, the seismic network is more likely to detect a greater proportion of the rockfall signals because the distance that the rockfalls cover is longer. Also, a larger and higher dome likely results in more energy being available to transfer to the ground for an equivalent rockfall volume on a smaller dome. It is also possible that the volume of individual rockfalls could increase as the dome increases in size, and this would not be reflected in the rockfall event counts data.

In Section 4.1.5, the average rates of carapace generated and talus readjusted for four different extrusion rates modelled are illustrated. The result was a linear relationship between average carapace generation rate and talus adjusted rate, against extrusion rate. But rockfall events for this dome growth period do not have a linear relationship to extrusion rate. This was shown by Loughlin et al. (2006) who compared the rockfall counts and energy throughout the dome growth episode with extrusion rates and observations.

Our simulation output data provides complete information regarding the development and readjustment of carapace/talus no matter how small or seismically undetectable these theoretical adjustments may be. A caveat however, is that the time-averaged extrusion rate used as an input, probably neglects short-time scale variations or pluses in magma influx which may be significant (Sparks et al., 1998). As a result, care is obviously required when interpreting the seismically detected data to our simulated data in Figure 14. For example, when the extrusion rate is low (and in this case the dome volume is small) seismically detected rockfalls as generated by talus adjustment are likely to be under-represented. Resolving the volume of talus material deformed using seismically-detected rockfalls is beyond the scope of this paper, but needs to be addressed for a better understanding of talus slope evolution.

4.2.5 Rockfall Volumes

Complicating the cumulative record of seismic rockfall signals further are the peaks in activity near days 85 and 115 (Fig. 14) due to brief pulses in magma supply. Ignoring these brief spurts in the number of rockfall seismic signals and biases in rockfall detection due to dome volume, our simulated cumulative volume of talus readjusted and volume of talus within the dome

provide reasonable fits to the seismic data-set. Equating the total number of detected rockfalls to the total volume of talus readjusted suggests that on average each rockfall would have a volume of between approximately 7,500 and 13,500 m^3 for the simulation parameters considered here. Assuming that the total rockfall number equates to the cumulative volume of carapace generated (i.e. total volume of talus), the volume per rockfall would have to be between approximately 3,100 and 7,800 m^3.

During an 11-day monitoring period (30th March – 11th April 2006) Wadge et al. (2008) calculated that the total increase in dome volume was approximately 9.0 $x10^6$ m^3 as measured by the radar instrument AVTIS. During this time period there were approximately 1040 rockfalls and 13 pyroclastic flows detected seismically, and thus an average of 96 rockfalls per day. This was a relatively active period in terms of rockfall generation, but this value is average for a primarily exogenous dome growth period (Calder et al., 2002). Assuming dome growth was accommodated entirely exogenously during this period (i.e. the growth volume of the talus apron, occurred solely by aggradation of new material on the surface, and not by internal inflation), then an average volume of talus aggraded per rockfall is calculated to be approximately 8,700 m^3 per rockfall. This value falls within our simulated average volume per rockfall for total talus readjustments, although we do not consider the conversion from dense rock equivalent to talus density.

4.2.6 Aseismic Talus Adjustment

The average volume per rockfall as measured by Calder et al. (2002) for SHV during dome growth in 1997 was 2,600±1,000 m^3. This figure was obtained using the talus volume of 25 x 10^6 m^3 for the southern talus apron measured in December 1999 (Sparks et al., 2002). The activity contributing to this accumulated talus apron was confined to two distinct periods, 10 Feb. - 14 May 1997 and 3 Nov. - 26 Dec. 1997. Dome collapses that occurred during these periods (30, 31 March, 11 April 1997, 4, 6 November 1997) were estimated to remove 8 x 10^6 m^3 of dome material, the remaining volume was divided by 6,070 (the total number of rockfalls that occurred in the two periods 10 Feb. - 14 May 1997 and 3 Nov. - 26 Dec. 1997. Growth of the southern talus apron occurred during a period when talus spilled over the rigid crater wall. This barrier would have prevented any lateral movement of the dome core and hence this volume must only

have recorded talus volume changes due to rockfalls and pyroclastic flows aggradation, and not any outward migration of the talus slope by internal spreading.

On average, for our simulations, each rockfall has a volume of 7,500 - 13,500 m^3 when calculated as the volume of talus readjusted, or 3,100 - 7,800 m^3 when calculated for the cumulative volume of carapace generated (equal to the total volume of talus within the dome). These values are considered relatively high based on the measurements explained above of 2,600±1,000 m^3. However, these estimates for individual rockfall volumes were obtained when talus spilled over a rigid crater wall and hence any internal expansion could be ruled out. This implies that an important component of the talus slope growth might occur by internal swelling of the core rather than by being deposited directly on the surface of the dome. Hence, our simulated talus readjusted volumes are significant because they suggest that substantial talus volume readjustment could occur either due to large volumes of seismically undetected rockfalls (considered unlikely), or aseismic creep due to a laterally spreading core bulldozing the talus.

Wadge et al. (2008) calculated that on average 8,700 m^3 per rockfall was aggraded to the talus slope during the time period 30th March – 11th April 2006, considerably more than the value of 2600±1000 m^3 per rockfall made by Calder et al. (2002). Assuming that the average volume of material shed during rockfalls has not changed with time, this suggests that a significant proportion, approximately 70%, of the volume of talus adjusted during dome growth could be generated from spreading of the core, i.e. aseismic talus adjustment. However, this value is unlikely to remain constant over the duration of dome growth. Hence, during the lava dome growth period considered in this paper it is possible that aseismic deformation of the talus could have occurred due to lateral spread of the core resulting in the large volume of talus per rockfall as predicted by our simulation. Also, at later times in the growth history of the dome it is likely to be largely pre-existing talus that is modified due to inflation and spreading of the core (i.e. endogenous behaviour), by an aseismic process of frictional adjustment between clasts within the talus.

4.2.7 Rockfall Seismicity Energy Data

To directly compare our simulation results (currently in volume form) to the energy proxy data for rockfall seismicity we must convert our simulated data into a pseudo-energy value. We achieve this by taking the product of the volume of dome material readjusted and half the maximum height from where the talus readjustments occur (R_a , Fig. 4a). This pseudo-energy can be considered to be proportional to the potential energy for the talus. In Figure 15 the cumulative energy as shown by the black circles, plotted with our simulated readjusted talus pseudo-energy a), and the carapace generated pseudo-energy b). The relationship between rockfall kinetic energy and seismic energy density is not yet established but again, will likely vary as the dome grows in size. For example, when the dome is small or the run-out constrained, the velocities achieved will tend to be lower than when the slope is longer. Therefore caution needs to be applied when drawing inferences from the comparison between the simulated data and the seismic energy data-set.

The gradient for cumulative energy data is relatively shallow initially, increase significantly but briefly around day 180, and then in a more sustained way between day 200 and day 250, before decreasing after day 260. Although not shown here, our companion paper Hale et al. (In review) shows that the maximum height at which talus readjustments occur increases as dome radius increases, except for when the dome is very large, and talus readjustment can occur lower on the flanks of the dome. This means that rockfalls may be sourced from lower locations on the dome surface, and these rockfalls have less potential energy to be converted into kinetic energy. However the overall decline in seismic energy leading up to 20 May was also documented by Loughlin et al (2006) and attributed to the fact that most rockfall activity was on the SW and W faces of the dome where rockfalls were stopped, after a short run-out, by the crater wall (Loughlin et al., in review). A decrease in seismic energy may be a combination of these two processes.

5. Discussion and Conclusions

Rockfall seismicity is the best available continuous proxy measurement we have for potentially distinguishing exogenous from endogenous dome growth. That is, the ratio of rockfall volume over equivalent-period extruded volume is a measure of the fractionation of the new lava into

solid core and clastic talus components and hence could be used to determine the different growth styles. Rockfall seismicity data could be used to track the relative contributions from both mechanisms provided the seismicity can be better calibrated to the rockfall volume and transport process. However, carapace disintegration and the formation of rockfalls is not as simple as suggested by our model. Our continuum model cannot represent discontinuous or non-equilibrium behaviour. For example, the highest average extrusion rates in this dome growth episode were recorded from 10 to 24 February (days 194 - 208) during emplacement of a pancake lobe characterised by low rockfall counts. Another form of such behaviour was measured by Wadge et al., (2008) between 5 and 7 April 2006. On 5 April the rockfall seismicity rate fell whilst at the same time the summit of the dome was observed to increase its height by about 20 m. After two days of low rockfall seismicity the rate picked up again on 7 April. This was interpreted as a pulse of exogenous lava addition to the summit, perhaps from a new lava lobe, which did not result in a renewed high level of rockfalls until the new lava had flowed to the edge of the relatively flat summit region and began another period of "equilibrium" disaggregation to produce the rockfall events. So whilst the model may successfully simulate the long-term pattern it fails to represent the short-term discontinuous, asymmetric and non-equilibrium aspects.

Despite not modelling the physics associated with exogenous dome growth explicitly, our model can replicate some of the large-scale behaviour associated with exogenous dome growth via a carapace generation mechanism. Exogenous growth is favoured when the viscosity of the talus is higher that that of the core, during higher extrusion rates, when the dome is small or when a large volume of talus surrounds the core. Determining regimes of dome growth is important for determining the stability of a lava dome. There were minimal precursory signals before the May 20th 2006 dome collapse event. Some of the models explored here provide a potential mechanical explanation for this. If the core had spread laterally over a layer of talus, which could have acted as a weak layer, focused rainfall runoff may have eroded this layer, triggering collapse. Such lateral spreading of the core could have been recorded by passive rockfalls originating low on the talus slopes.

Results for our generic lava dome growth model show that the core has the potential to grow larger when extrusion rates are low (aided by gravitational spreading) compared to domes with higher extrusion rates. This will result in the talus being deformed to a greater degree laterally in an aseismic fashion and the production of fewer rockfalls from freshly extruding carapace. Seismic data show that, in general, low extrusion rates generate fewer rockfall signals and that the frequency-magnitude curve for rockfalls shifts at higher extrusion rates (Calder et al., 2005). Further, for an upwardly growing dome (i.e. exogenous growth) it is likely that more rockfalls will be generated because this upward motion of lava is likely to generate larger regions of the dome surface which are at angles greater than the talus angle of repose (dominantly active rockfalls). While a dome with a wide core is likely to have a flatter central region and hence a smaller area with angles close to or greater than the talus angle of repose meaning an inflating (endogenous) dome is more likely to generate dominantly passive rockfalls.

The most novel result to come from this work is the prediction of the degree of internal deformation that might occur at the core-talus boundary and how we might test our results. Unfortunately, the 2005-2006 dome no longer exists. But at SHV there are a few other pieces of observational evidence that we can use to better understand whether the core-talus interface can evolve as suggested in some of our models The location of core remnants after the 2003 dome collapse at distances of about 200 m from the conduit exit indicate that the core must have extended at least as far as that. Earlier, partially-collapsed domes at SHV show massive jointed lava in the core but no real evidence of a pronounced bulge of core lava at lower levels with evidence of overriding of talus. But of course this is exactly the part of the dome that gets destroyed most readily in major collapses, so absence of evidence in this case cannot be taken as evidence of absence.

Improved accounting of the rockfall process using integrated seismicity and radar survey type techniques such as AVTIS or LIDAR (Wadge et al., 2008) could provide observational evidence for or against the process of core spreading. More accurate estimates of individual rockfall volumes together with a better understanding of talus packing during burial is needed. Phenomena such as the initiation of a band of minor passive rockfalls from lower down on the talus could indicate the surface effects of lateral spread as suggested by our model. However,

local passive rockfalls forced by the internal deformation may mask any surrounding surface topographic expression and/or rockfalls from higher on the dome may do likewise. The shape and rate of such surface deformations should help to infer source mechanisms, for example between lateral/downslope spread and upward intrusion of a shear-bounded body.

During exogenous dome growth, lava is channelled to the free-surface, which can result in talus being almost entirely derived from rockfalls at the dome surface. This energetic process can result in the talus resting at below its critical angle of repose due to a kinematic component (Lube et al., 2005). However, during endogenous inflation of the core, the adjustment of the talus is much more gradual, meaning that talus adjustments are likely to be relatively small and the slope will depart minimally from the critical angle of repose.

Acknowledgments. Support is gratefully acknowledged from the Australian Research Council Discovery grant DP0771377 and AJH also acknowledges a University of Queensland Early Career Research Grant. ESC acknowledges NSF funding (Grant Number 0809543) as well as a UB2020 Scholars grant. SCL publishes with permission of the Executive Director of BGS (NERC). Thanks to the continued efforts of scientists and staff at the Montserrat Volcano Observatory without which this work would not have been possible. GW is supported by NERC grant NE/E015093/1.

References:

Barclay, J., M. J. Rutherford & M. R. Carroll, 1998. Experimental phase equilibria constraints on pre-eruptive storage conditions of the Soufriere Hills magma, *Geophys. Res. Lett.,* **25**, 3437 - 3440.

Calder, E. S., Luckett, R., Sparks, R. S. J., & Voight, B., 2002, The eruption of Soufriere Hills Volcano, Montserrat from 1995 to 1999. *Geological Society, London Memoir*, **21**, 173–190.

Calder E. S., Cortes J. A., Palma J. L. & Luckett R., 2005. Probabilistic analysis of rockfall frequencies during an andesite lava dome eruption: The Soufriere Hills Volcano, Montserrat, *Geophysical Research Letters*, **32**, L16309

Calder, E.S. and Bernstein, M., 2007. Dome Collapse Inventory, 1996-2008. MVO Open File Report OFR06-09

Gross, L.,. Bourgouin L, Hale A. J., & Mühlhaus H.-B., 2007. Interface Modeling in Incompressible Media using Level Sets in Escript, *Physics Earth Planet. Int*., **163**, 23–34

Hale, A. J., Calder, E. S., Loughlin, S., & Wadge, G.,. Modelling the Lava Dome Extruded at Soufriere Hills Volcano, Montserrat, August 2005 - May 2006. Part I: Dome Shape and Internal Structure. *(submitted)*

Hale, A. J., 2008. Lava Dome Growth and Evolution with an Independently Deformable Talus. *Geophysical Journal International.* **174,** 391–417

Hale, A. J. & Wadge, G., 2008. The transition from endogenous to exogenous growth of lava domes with the development of shear bands. *Journal of Volcanology and Geothermal Research,* **171,** 237–257.

Hale, A. J., Bourgouin L., & Mühlhaus H.-B. 2007. Using the level set method to model endogenous lava dome growth, *J. Geophys. Res*., **112**, B03213 doi:10.1029/2006JB004445.

Jolly, A. D., Thompton, G. & Norton, G. E., 2002. Locating pyroclastic flows on Soufriere Hills Volcano, Montserrat, West Indies, using amplitude signals from high dynamic range instruments. *Journal of Volcanology and Geothermal Research*. **118**, 299 - 317.

Jones, L. D. (2006), Monitoring landslides in hazardous terrain using terrestrial LiDAR: an example from Montserrat. , Quarterly Journal of Engineering Geology and Hydrology, 39, 371-373.

Lavallée, Y., Hess, K.-U., Cordonnier, B. & Dingwell, D. B., 2007. Non-Newtonian rheological law for highly crystalline dome lavas. *Geology*, **35** 843 – 846

Loughlin, S. C., Calder, E. S., Clarke, A., Cole. P. D., Luckett, R., Mangan, M. T., Pyle, D. M., Sparks, R. S. J., Voight, B. & Watts R. B. 2002. Pyroclastic flows and surges generated by the 25 June 1997 dome collapse, Soufriere Hills Volcano, Montserrat. Geological Society Memoir **21**, 191-209.

Loughlin, S. V., Christopher, T., Luckett, R., Jone, L., Baptie, B., 2007. Large volume dome collapse at the Soufrière Hills Volcano, Montserrat, 20 May 2006. *Geophysical Research Abstracts*. **9**, 11090.

Loughlin, S. V., Baptie, B, Christopher, T., Ryan, G., Luckett, R., Hards, V., Jones, L., Fournier, N., Bass, V., Syers, T., Ruzie, L., Higgings, M., Williams, P & Williams, D., 2006. *Report to the Scientific Advisory Committee Montserrat, August 2006. MVO Open File Report 06/07*.

Loughlin, S. C., Luckett, R., Christopher, T., Jones, L., Ryan, G., Druitt, T., Baptie, B., Carn, S., Hards, V. 2009. Unprecedented gas release from a large volume and rapid dome collapse at Soufriere Hills Volcano, Montserrat on 20 May 2006. Journal of Volcanology and Geothermal Research. In prep.

Luckett, R., Baptie, B. & Neuberg, J., 2002. The relationship between degassing and rockfall signals at Soufriere Hills Volcano, Montserrat. *Geol. Soc. London, Memoir,* **21**, 595-602.

Lube, G., Huppert, H. E., Sparks, R. S. J., & Freundt, A., 2005. Collapse of two-dimensional granular columns. *Physical Review E*. **72**, 041301.

Ryan, G. A., Loughlin, S. C., James, M. R., Jones, L. D., Calder, E. S., Christopher T., Strutt, M. H. & Wadge , G. (in prep.). Growth of the lava dome and magma extrusion at Soufriere Hills Volcano, Montserrat, West Indies: 2005-2008.

Simmonds, J., Elsworth D.& Voight B. 2005. Classification and idealized limit-equilibrium analyses of dome collapses at Soufrière Hills volcano, Montserrat, during growth of the first lava dome: November 1995–March 1998. *J. Volc. Geotherm. Res*., **139**, 241–258.

Sparks, R. S. J., Young, S. R., Barclay, J., Calder, E. S., Cole, P., Darroux, B., Davies, M. A., Druitt, T. H., Harford, C., Herd, R., James, M., Lejeune, A. M., Loughlin, S., Norton, G., Skerrit, G., Stasiuk, M. V., Stevens, N. S., Toothill, J., Wadge, G., & Watts, R. 1998. Magma production and growth of the lava dome of the Soufriere Hills Volcano, Montserrat, West Indies: November 1995 to December 1997. *Geophysical Research Letters.* **25**, 3421 - 3424

Sparks, R. S. J., M. D. Murphy, A. M. Lejeune, R. B. Watts, J. Barclay & S. R. Young, 2000. Control on the emplacement of the andesitic lava dome of the Soufrière Hills Volcano, Montserrat by degassing-induced crystallisation. *Terra Nova*, **12**, 14 - 20.

Sparks, R. S. J. & Young, S. R., 2002. The eruption of Soufrière Hills Volcano, Montserrat (1995 - 1999): overview of scientific results. *Geological Society, London Memoir*, **21**, 45 - 69.

Uhira et al., 1994. K. Uhira, H. Yamasato & M. Takeo , Source mechanism of seismic waves excited by pyroclastic flows observed at Unzen volcano, Japan. *J. Geophys. Res.* **99** (1994), 17757–17773.

Ui, T., Matsuwo, N., Sumita, M. & Fujinawa, A., (1999). Generation of black and ash flows during the 1990 – 1995 eruption of Unzen Volcano, Japan. *Journal of Volcanology and Geothermal Research*. **89**. 123 – 137.

Voight, B., 2000. Structural stability of andesite volcanoes and lava domes. *Phil. Trans. Royal Soc. Lon. A*, **358**, 1663–1703

Wadge, G., 2008. Assessing the pyroclastic flow hazards at Soufriere Hills Volcano, Montserrat. In*: Advances in Volcanology: the Legacy of G. P. L. Walker, Geol. Soc. London* (*in press*).

Wadge G, Macfarlane D. G., Robertson D. A. Hale, A. J., et al. 2005. AVTIS: A novel millimetre-wave ground based instrument for volcano remote sensing. *Journal of Volcanology and Geothermal Research.* **146**, 307-318.

Wadge, G., MacFarlane, D. G., Odbert, H. M., James, M. P., Hole, J. K., Ryan, G., Bass, V., De Angelis, S., Pinkerton, H., Robertson, D. A. & Loughlin, S. C., 2008. Lava dome growth and mass wasting measured by a time series of ground-based radar and seismicity observations. *Journal of Geophysical Research*, **113**, B08210, doi.1029/2007JB005466.

Wadge, G., Ryan, G. & Calder, E. S. (2008b). Clastic and core lava components of a silicic lava dome. Geology (submitted).

Watts, R. B., R. A. Herd, R. S. J. Sparks & S. R. Young, 2002. Growth patterns and emplacement of the andesitic lava dome at Soufrière Hills Volcano, Montserrat, *Geological Society, London Memoir,* **21**, 115 - 152.

Yamamoto, T., Takarada, S. & Suto, S., 1993. Pyroclastic flows from the 1991 eruption of Unzen volcano, Japan. *Bull. Volcanol.* **55**, 166–175.

Zobin, V.M., 2003. Introduction to Volcanic Seismology: Developments in volcanology 6, Elsevier.

Figure Captions

Figure 1: a) Boundary conditions used in the model. The model domain has an axis of symmetry about r = 0 and this allows us to only model a 2D slice, reducing computing solving time. The base of the domain has the boundary conditions of no-slip (as shown by the fixed triangle symbol), the axis of symmetry at r = 0 permits flow only in the z-direction (shown by the triangle on rollers), while the boundaries away from r = 0 and z = 0 are open and allow matter to flow in/out of the domain. Magma is introduced into the model domain through a conduit with radius a. The free-surface of the dome and the core-talus interface are described by level-sets. b) shows a typical mesh (grey lines) and the surfaces for the core-talus interface and free-surface (both black). Image c) shows profiles of a simulated lava dome (free-surface shown as grey lines and core-talus interface shown as black lines) at 5 different times. The region below the core-talus interface (black line) is the dome core. The black dots correspond to the point at which the free-surface departs from the talus angle of repose and the grey shaded region can be classified as carapace in our model, while the non-shaded region between the core-talus (black line) interface and dome free-surface (grey line) is identified as talus.

Figure 2: Surveyed dome volume data with time (crosses) and, on the secondary y-axis, the extrusion rate interpolated from the surveyed volume data (filled circles). Also shown are best-fit curves to the dome volume data (continuous line) and the extrusion rate curve derived from the best-fit curve for the volume (dashed line).

Figure 3: Radius and height for the generic lava dome model for a Newtonian viscosity (a and c), and for a shear-thinning viscosity model (b and d). There is negligible difference in dome height and radius between these different viscosity relationships when plotted against dome volume. Also, due to the common free-surface constraint for the talus readjustment, the dome shape is self-similar for these simulations.

Figure 4: a) Schematic of the lava dome model (a 270° rotated axi-symmetrical model with cut-away) during the talus readjustment sub-step. Following the injection of new lava into the core, the free-surface angle is calculated. The distance R_a corresponds to the minimum radius where

the dome surface is at an angle greater than the angle of repose. The free-surface of the talus is therefore adjusted to its angle of repose during the talus free surface adjustment sub-step, which may involved the readjustment of material from $0 > r > R_a$. Also shown is the talus readjustment volume, or talus source volume, shaded as grey. This corresponds to the volume of carapace/talus adjusted downslope so that the talus rests at angles below its angle of repose. b) Schematic showing the rockfall source volume (corresponding to a volume of over-steepened material close to the summit), analogous to the talus source volume as shown in (a). The aggraded talus is distributed along the flanks of the dome.

Figure 5: Variation of R_a/R for the generic dome models as they grow, using a) the Newtonian , and b) the shear-thinning viscosity relationships. The key corresponds to the extrusion rates applied for each of the four model runs. (c) shows a cartoon of how the dome shape may change depending upon the ratio, R_a/R. When $R_a/R \approx 0$, R_a is very small the dome shape is approximately conical. When $R_a/R \approx 1$, R_a is large relative to R, and the dome shape will tend to a truncated cone with a convex top.

Figure 6: Rate of talus readjusted for a Newtonian viscosity model (a), and a shear thinning (Lavallée et al., 2007) viscosity model (b). The key corresponds to the extrusion rate applied for each of the 4 model runs. Results are smoothed with a 100 time-step running average.

Figure 7: Schematic of the lava dome model showing the volume of new carapace generated from core. Carapace/talus is generated when core material moves into regions of the dome that are at a pressure below the solidus pressure, as shown by the dashed line.

Figure 8: Rate of carapace generated for the duration of the generic lava dome simulations with a Newtonian viscosity model, (a), and a shear thinning viscosity model (b). The key corresponds to the extrusion rate applied for each of the 4 model runs. Results are smoothed with a 100 time-step running average.

Figure 9: Average rates of carapace generated and talus readjusted at four extrusion rates for a Newtonian viscosity model (a) and a shear-thinning viscosity model (b). Note that the carapace generation rate is systematically lower than the talus readjustment rate since the latter includes material already within the talus apron that continues to deform.

Figure 10: Cumulative core volume fraction plotted against total dome volume for a Newtonian viscosity model (a), and a shear-thinning viscosity model (b). c) Profiles of lava dome free-surfaces and core-talus interfaces for a dome volume of 11.5 million cubic metres using a shear thinning viscosity model. Black lines are for the simulation with an extrusion rate of 8 m^3s^{-1} , while the grey lines are for the simulation with an extrusion rate of 2 m^3s^{-1}. d) the same profiles using shear thinning viscosity model (grey lines) and a Newtonian viscosity model (black lines) for a simulation with an extrusion rate of 8 m^3s^{-1}.

Figure 11: Simulated rate of carapace generated for the 292 days of growth of the August 2005 – May 2006 lava dome at SHV (a), and the ratio of this parameter with the extrusion rate (b), for eight different simulations with parameters sets as described in Table 3. c) Illustrates the proportion of core converted into carapace that is subsequently available to generate talus (therefore comparable to seismic rockfall data), and the proportion of core which simply spreads into regions of the dome, where pressure remains above the solidus pressure (and thus remain as core).

Figure 12: Simulated rate of talus adjusted for the 292 days of growth of the August 2005 – May 2006 lava dome at SHV (a), and the ratio of this parameter with the extrusion rate (b), for eight different simulations with parameters sets as described in Table 3.

Figure 13: A schematic taxonomy of rockfall events likely to occur at silicic lava domes. RF and PF stand for rockfall and pyroclastic flow events. The two schematic plots show possible relationships between number of events (left) and energy of individual events (right) against volume of rockfall event.

Figure 14: a) Simulated cumulative volume of talus readjusted compared to the cumulative number of rockfalls as measured by the seismic network during this dome growth period and . b) shows the simulated cumulative volume of carapace generated during the dome growth period, which represents the total volume of talus within the lava dome generated from gravitational collapse of the carapace, compared to the cumulative number of rockfalls measured during this dome growth (black circles).

Figure 15: a) Simulated cumulative proxy-energy for the volume of talus readjusted compared to the cumulative energy proxy for rockfalls as measured by the seismic network during this dome growth period. b) shows the simulated cumulative proxy-energy of carapace generated during the dome growth period, compared to the cumulative energy proxy for rockfalls measured during this dome growth (black circles).

Tables:

Table 1: Percentage of dome material extruded converted into carapace or readjusted talus.

	Viscosity model	2 m^3/s	4 m^3/s	6 m^3/s	8 m^3/s
Carapace generated	Newtonian	80%	83%	81%	83%
Carapace generated	Shear-thinning	68%	70%	69%	68%
Talus readjustment	Newtonian	98%	107%	112%	110%
Talus readjustment	Shear-thinning	99%	93%	95%	97%

Table 2: Parameters used in simulations.

Parameter	Range	Value used	Reference
θ (Friction angle)	33 – 43.5º	37 – 43.5º	Wadge et al. (2008)
ρ (Density – core and talus)		2350 kg m^3	
r_a (Conduit radius)		15 m	
P_s (Solidus pressure)	0.2 M Pa - 15 M Pa	0.2 MPa – 0.6 MPa	
T (Temperature)	830±10ºC in magma chamber	830ºC	Barclay et al., (1998)

Table 3: Simulations modelled.

Simulation	Viscosity model	Friction angle	Solidus pressure
1	Shear-thinning viscosity relationship (Lavallée et al., 2007) with strain-rate cut-off of 10^{-5} s^{-1}.	43.5º	0.2MPa
2	Shear-thinning viscosity relationship (Lavallée et al., 2007) with strain-rate cut-off of 10^{-5} s^{-1}.	43.5º	0.4MPa
3	Shear-thinning viscosity relationship (Lavallée et al., 2007) with strain-rate cut-off of 10^{-5} s^{-1}.	43.5º	0.6MPa
4	Shear-thinning viscosity relationship (Lavallée et al., 2007) with strain-rate cut-off of 10^{-5} s^{-1}.	40.0º	0.4MPa
5	Shear-thinning viscosity relationship (Lavallée et al., 2007) with strain-rate cut-off of 10^{-5} s^{-1}.	37.0º	0.4MPa
6	Shear-thinning viscosity relationship (Lavallée et al., 2007) with strain-rate cut-off of 10^{-5} s^{-1} for the core, and a viscosity of $3.4x10^{13}$ Pa s for the talus.	43.5º	0.4MPa
7	Shear-thinning viscosity relationship (Lavallée et al., 2007) with strain-rate cut-off of 10^{-5} s^{-1} for the core, and a viscosity of 10^{14} Pa s for the talus.	43.5º	0.4MPa
8	Newtonian viscosity relationship, $3.4x10^{12}$ Pa s.	43.5º	0.4MPa

Figure 1
Click here to download Figure: Fig1.pdf

Figure 1:

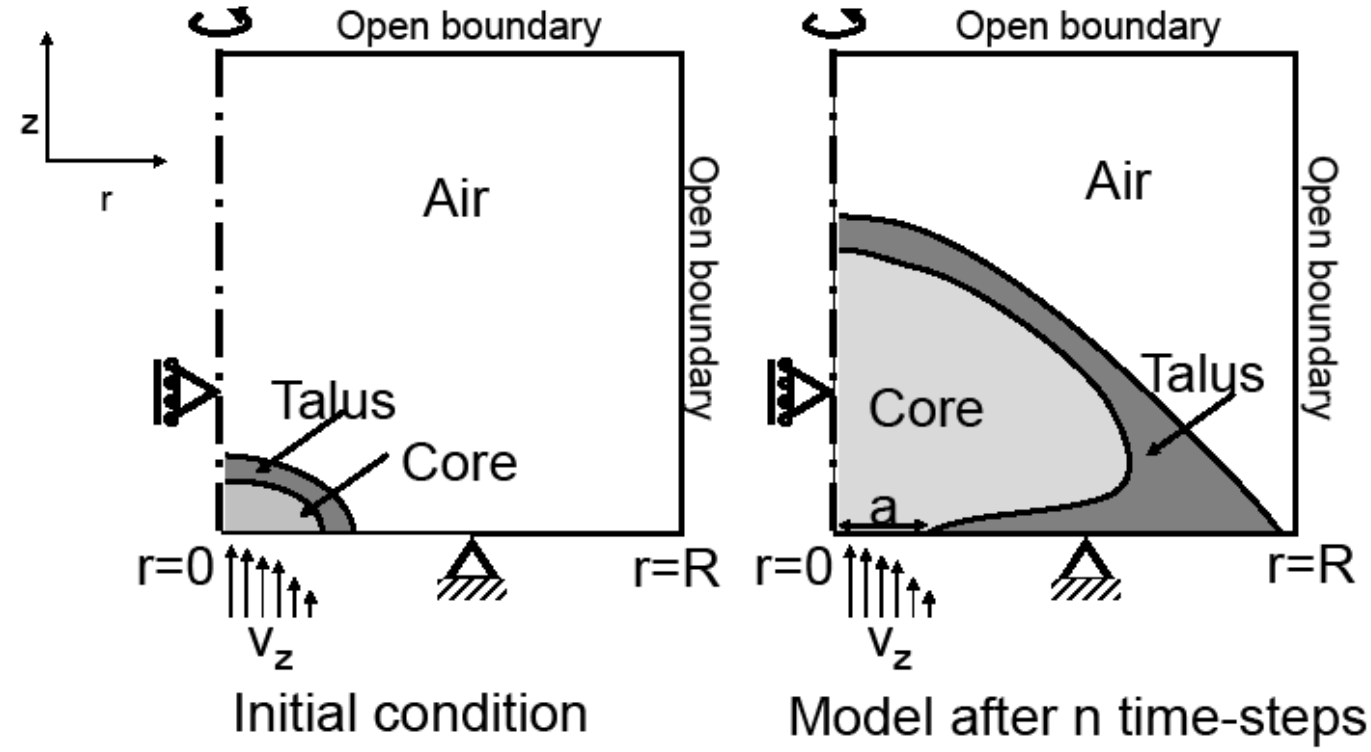

a)

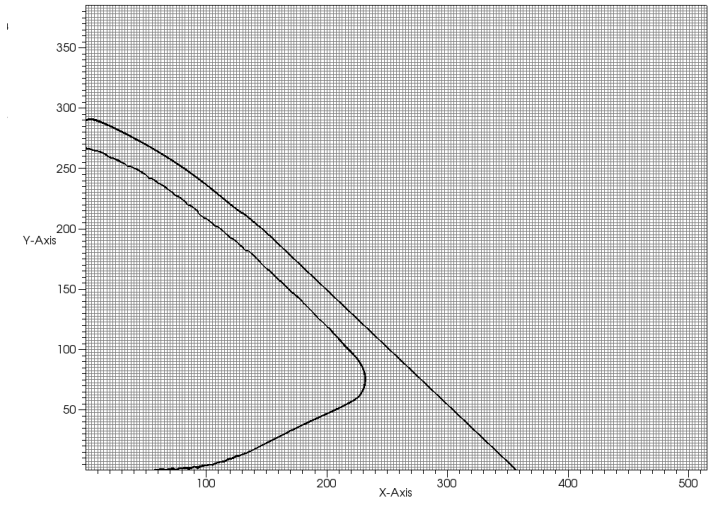

b)

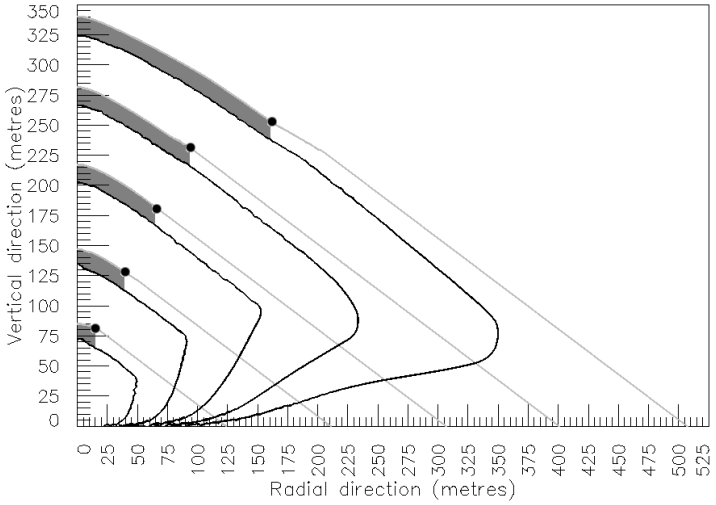

c)

Figure 2

Click here to download high resolution image

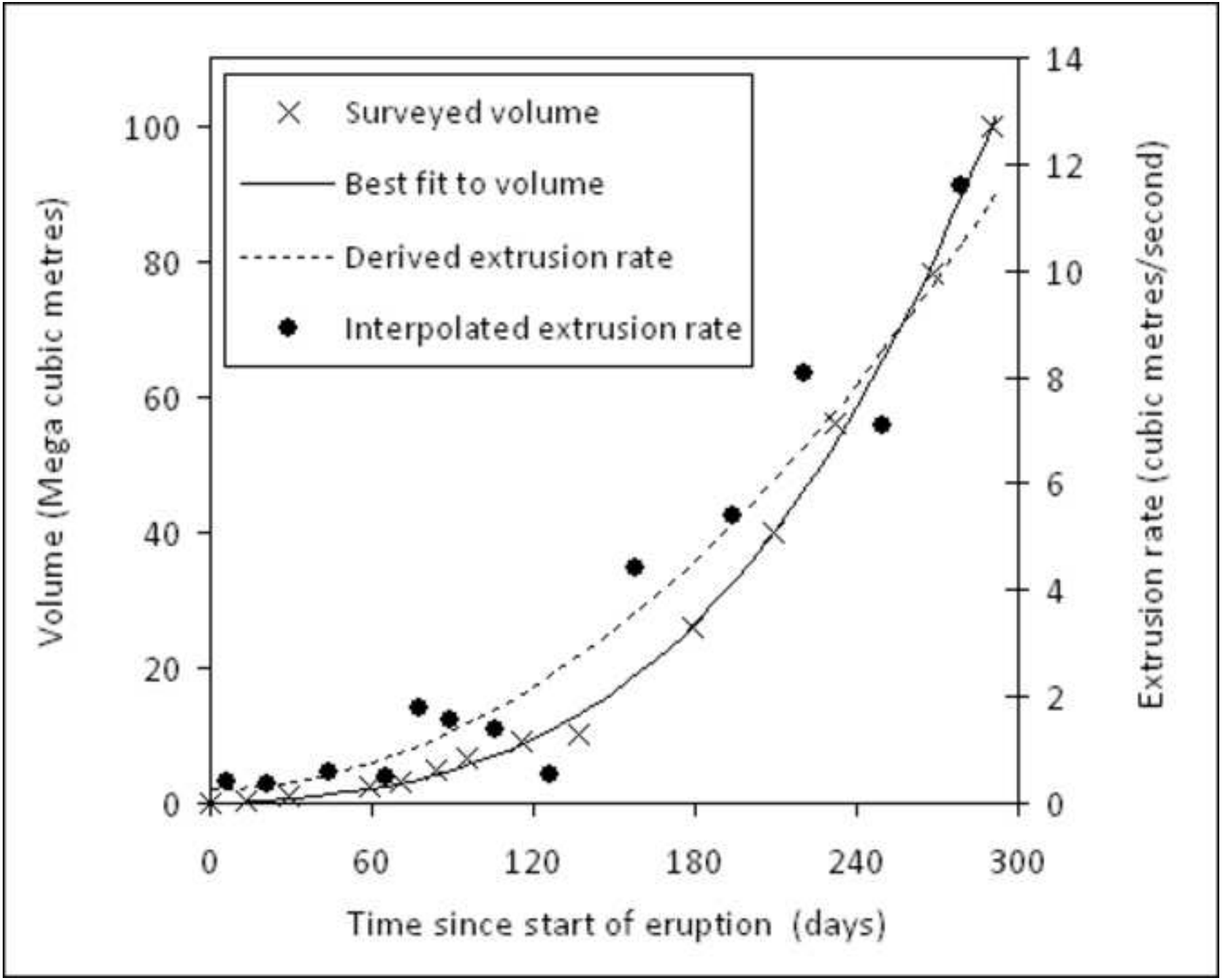

Figure 3
Click here to download Figure: fig3.pdf

Figure 3:

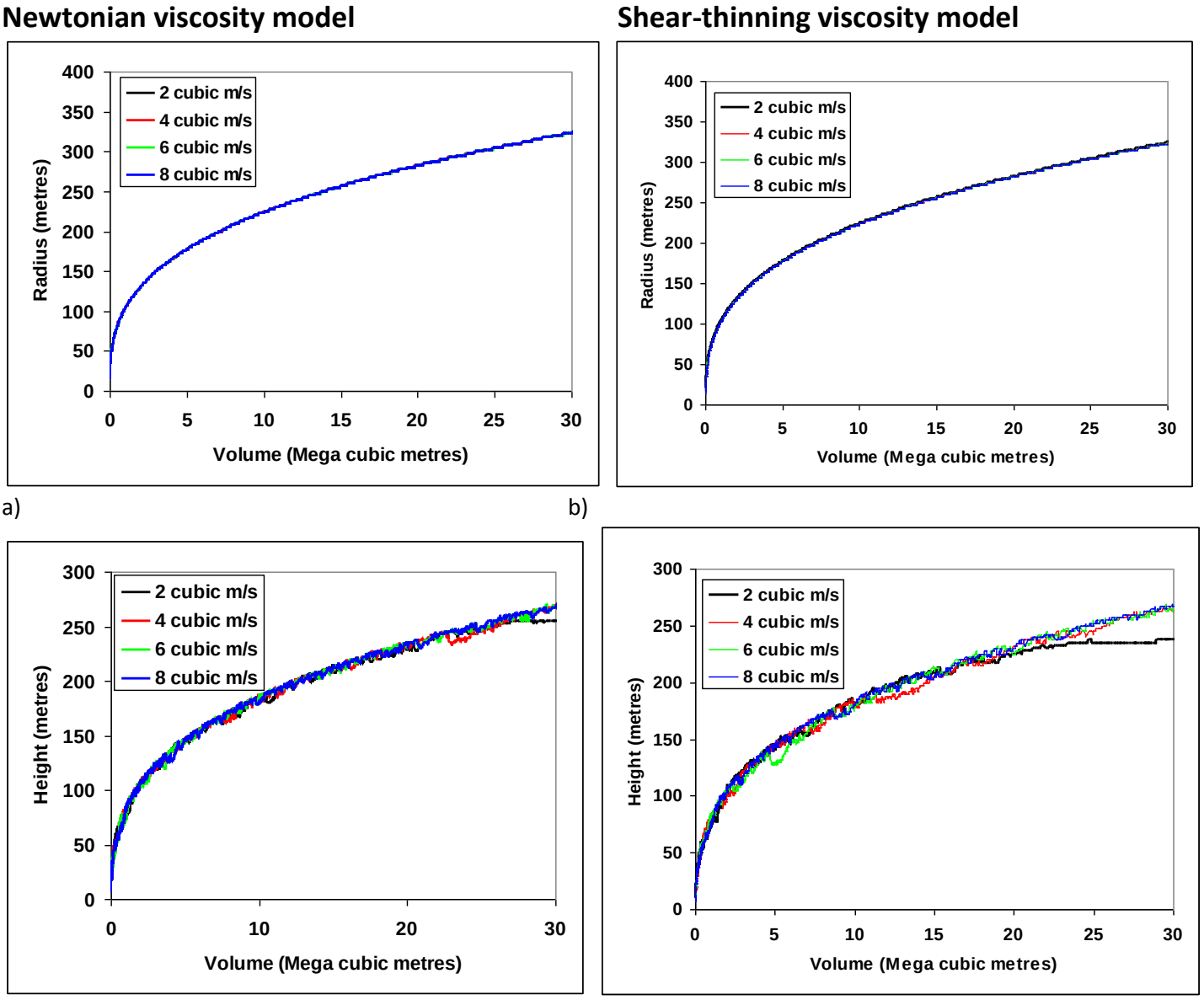

Figure 4a
Click here to download Figure: Fig4a_TalusAdj.pdf

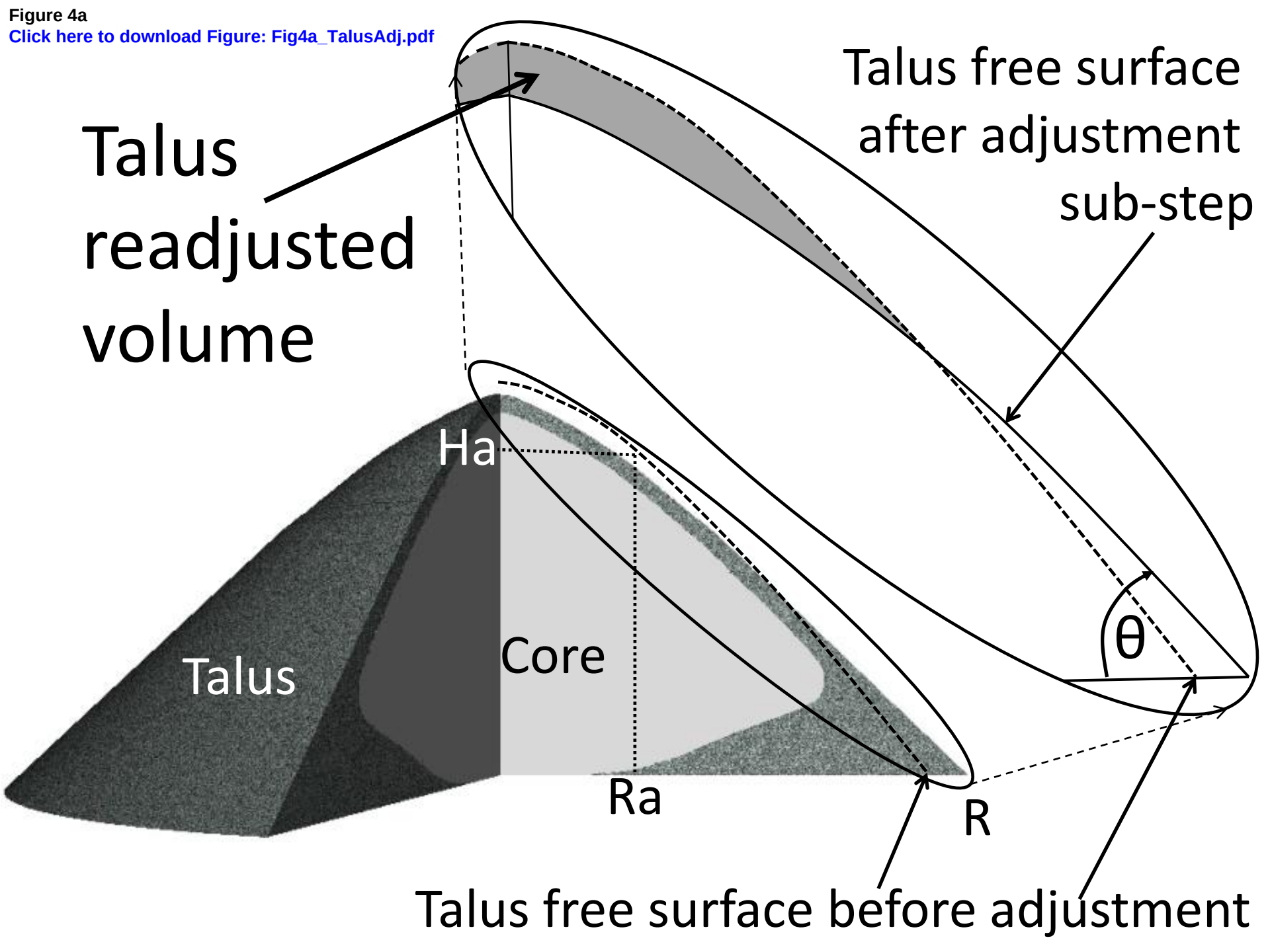

Figure 4b

Click here to download Figure: Fig4b_RockfallVol.pdf

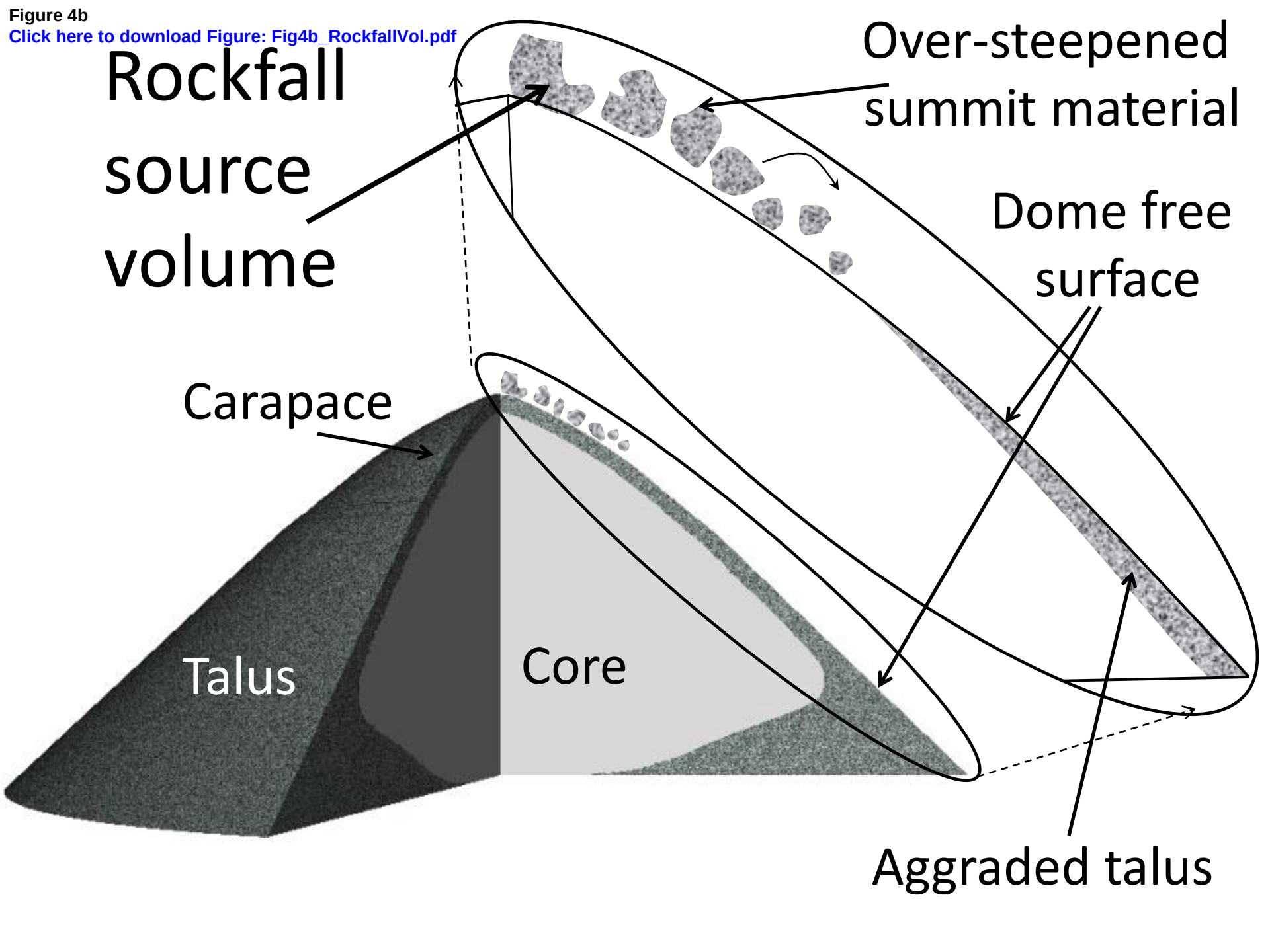

Figure 5
Click here to download Figure: Fig5.pdf

Figure 5:

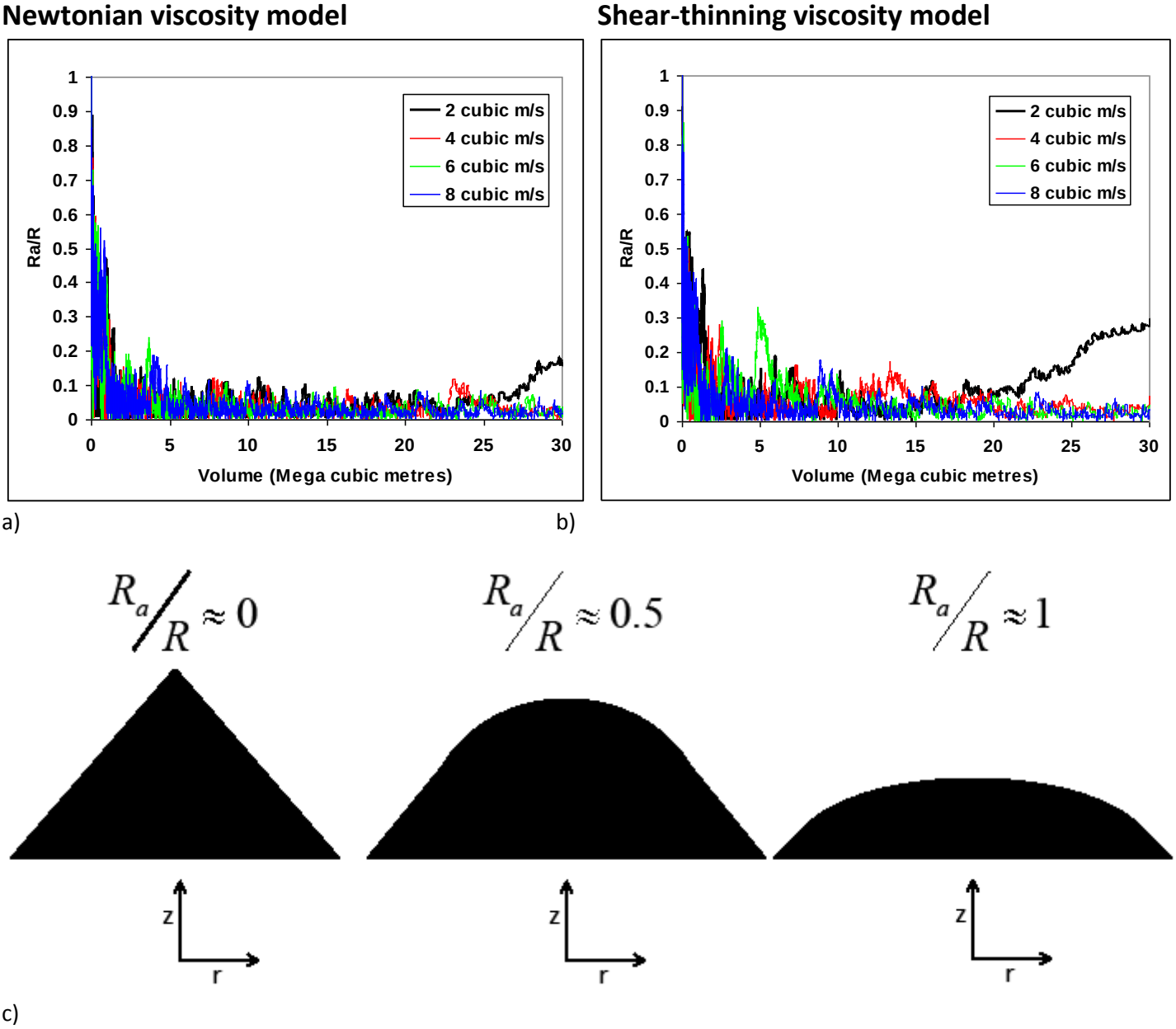

Figure 6

Click here to download Figure: Fig6.pdf

Figure 6:

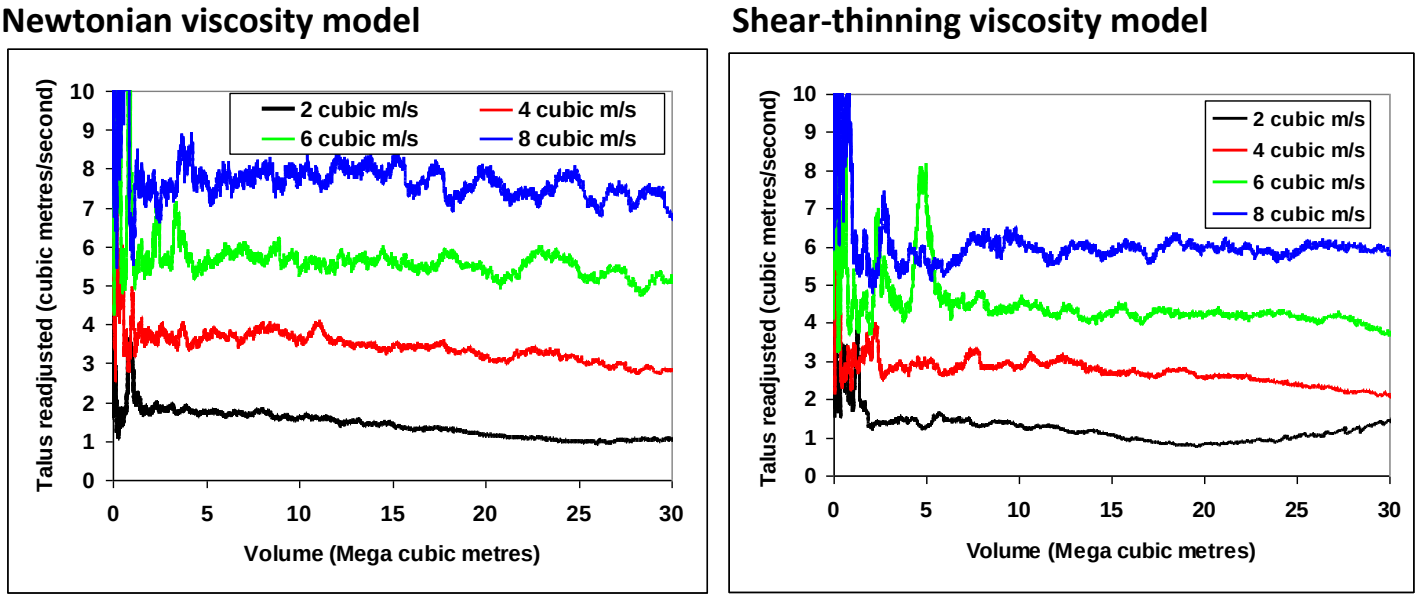

a) b)

Figure 7
Click here to download Figure: Fig7_CoreVol.pdf

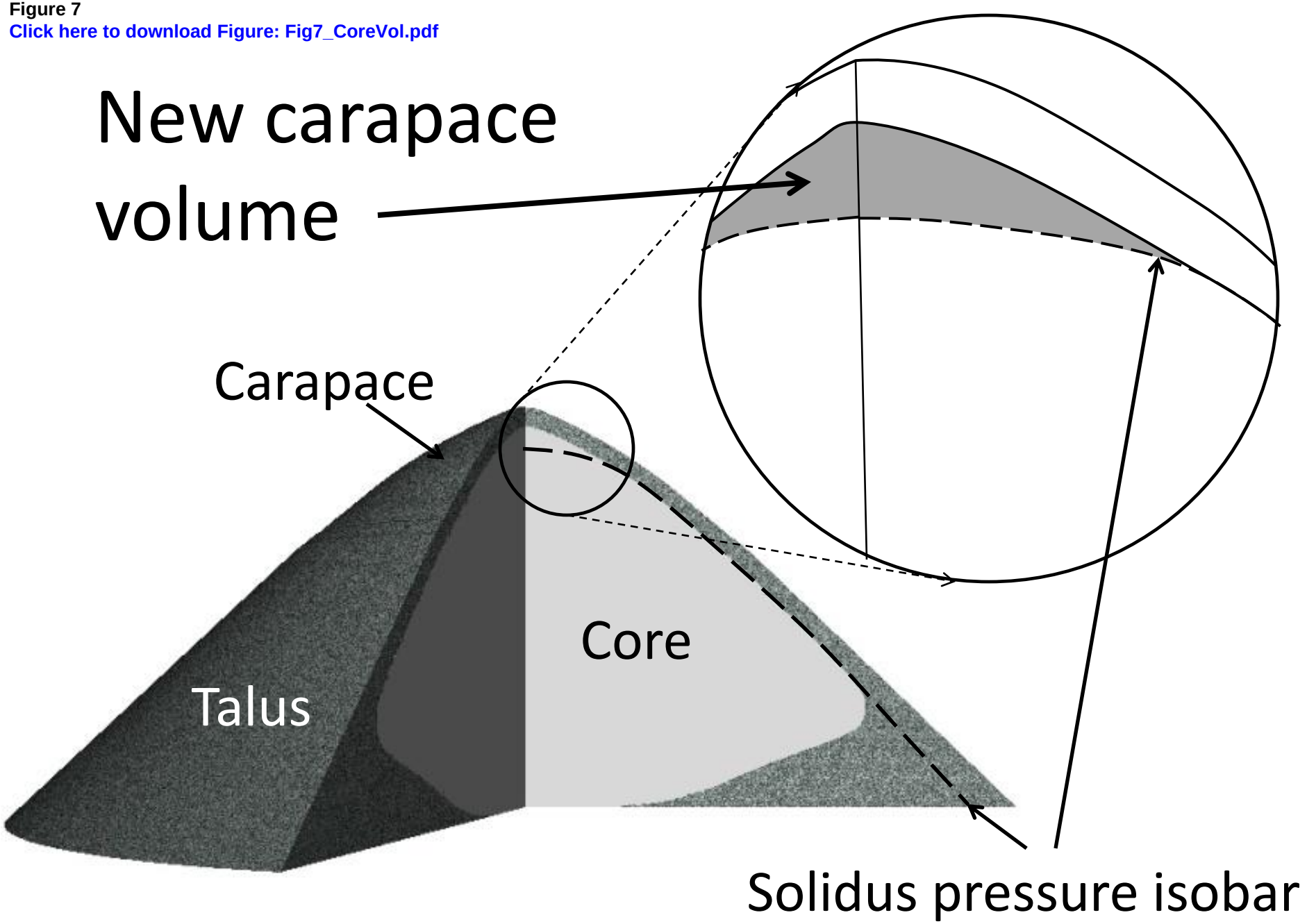

Figure 8

Click here to download Figure: fig8.pdf

Figure 8:

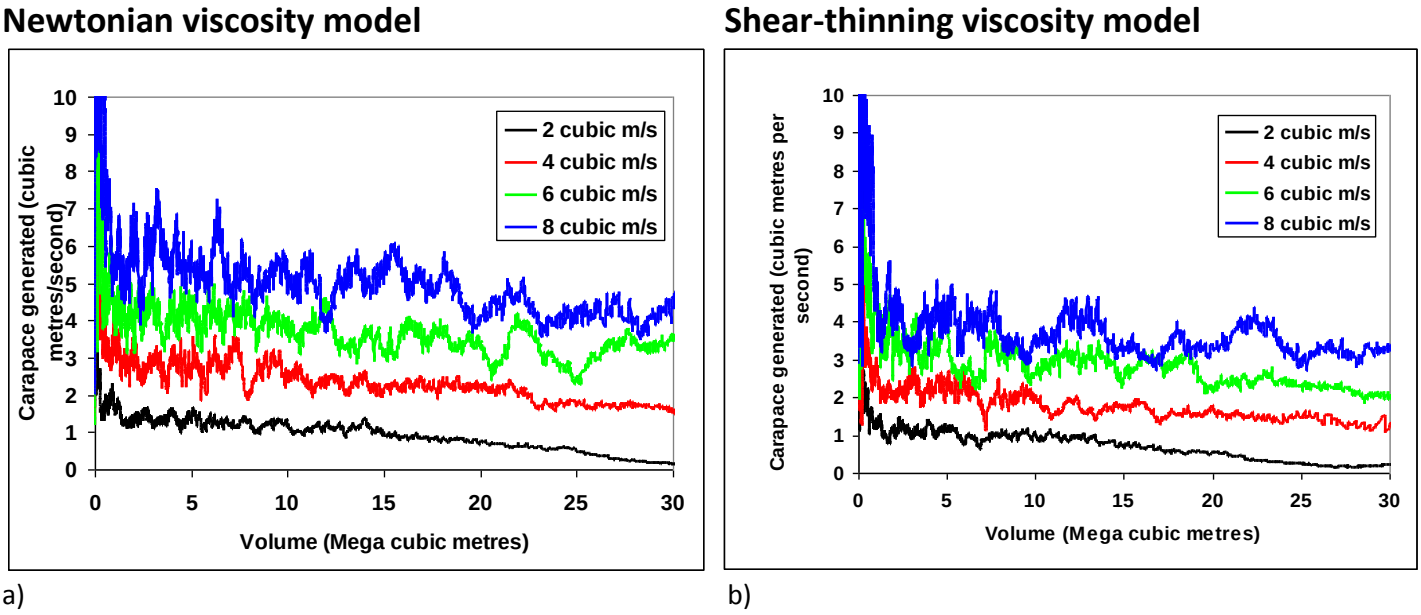

a)

b)

Figure 9
Click here to download Figure: Fig9.pdf

Figure 9:

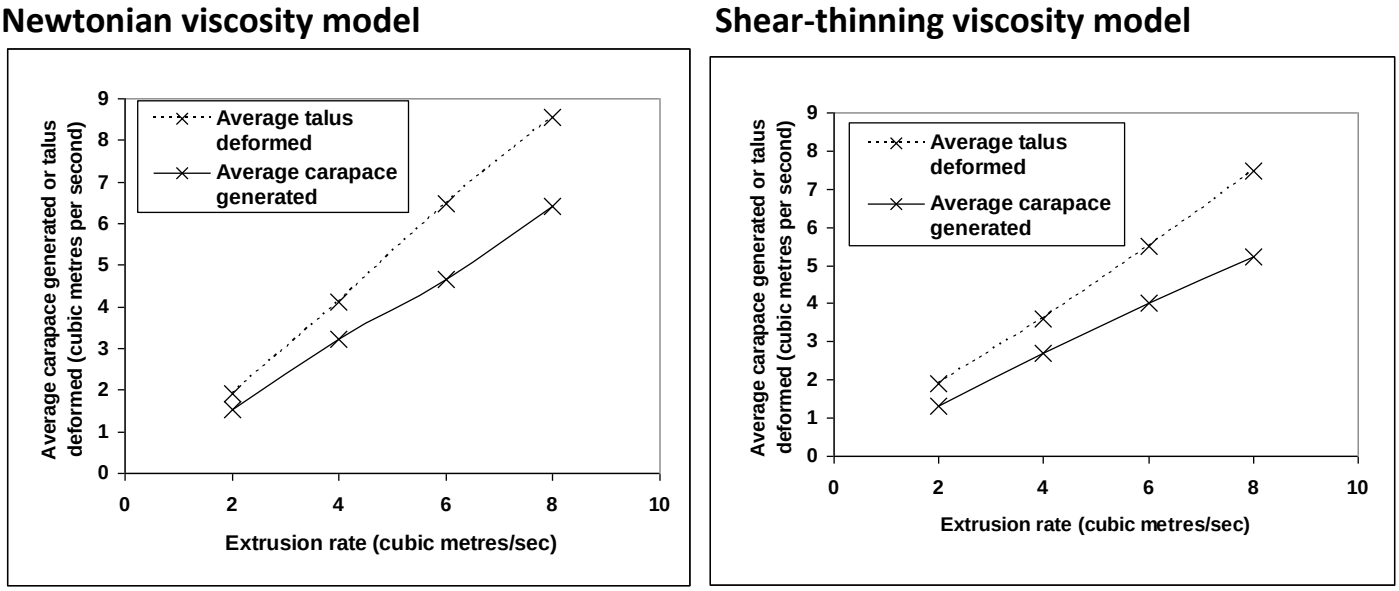

a) b)

Figure 10
Click here to download Figure: Fig10.pdf

Figure 10:

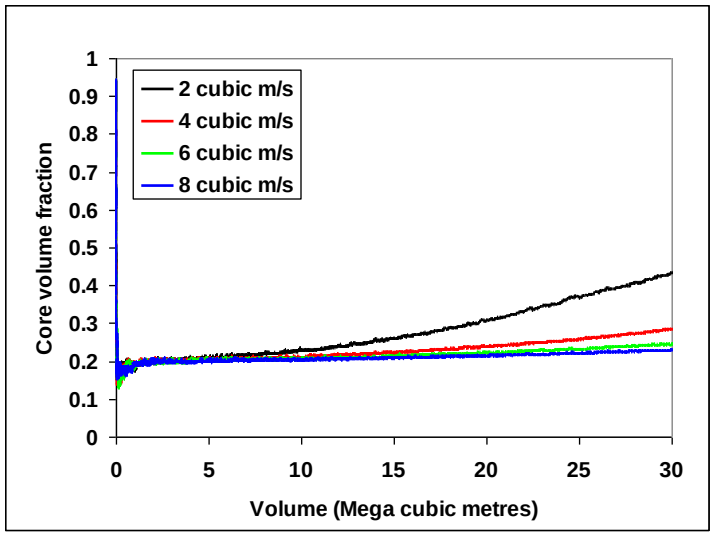

a) **Newtonian viscosity model**

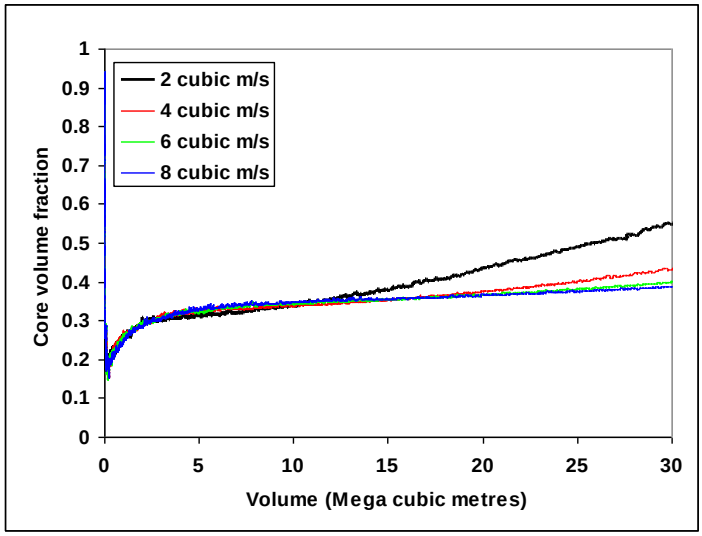

b) **Shear-thinning viscosity model**

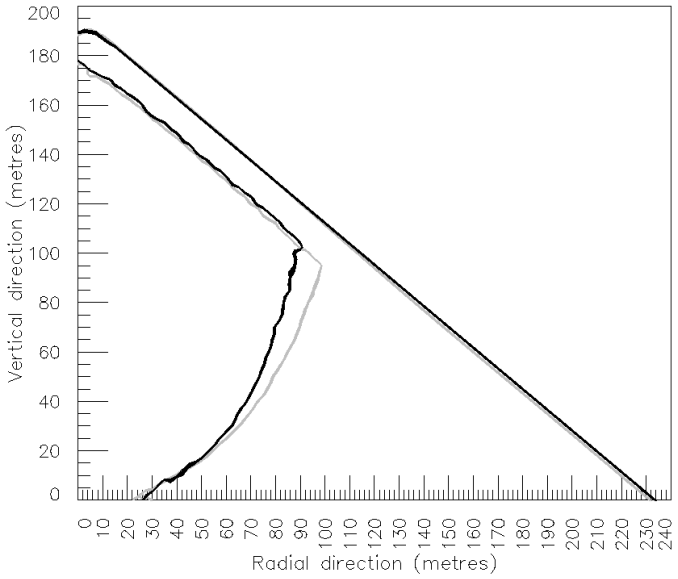

c)

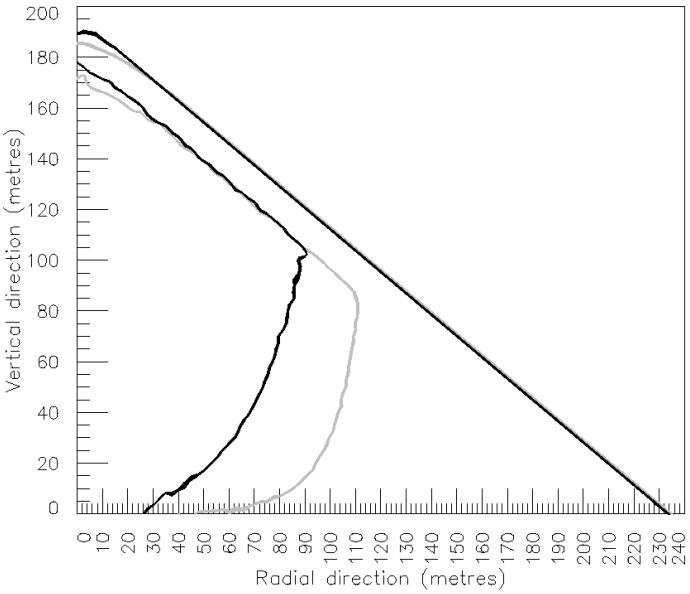

d)

Figure 11 a and b

Click here to download Figure: fig11_a&b.pdf

Figure 11:

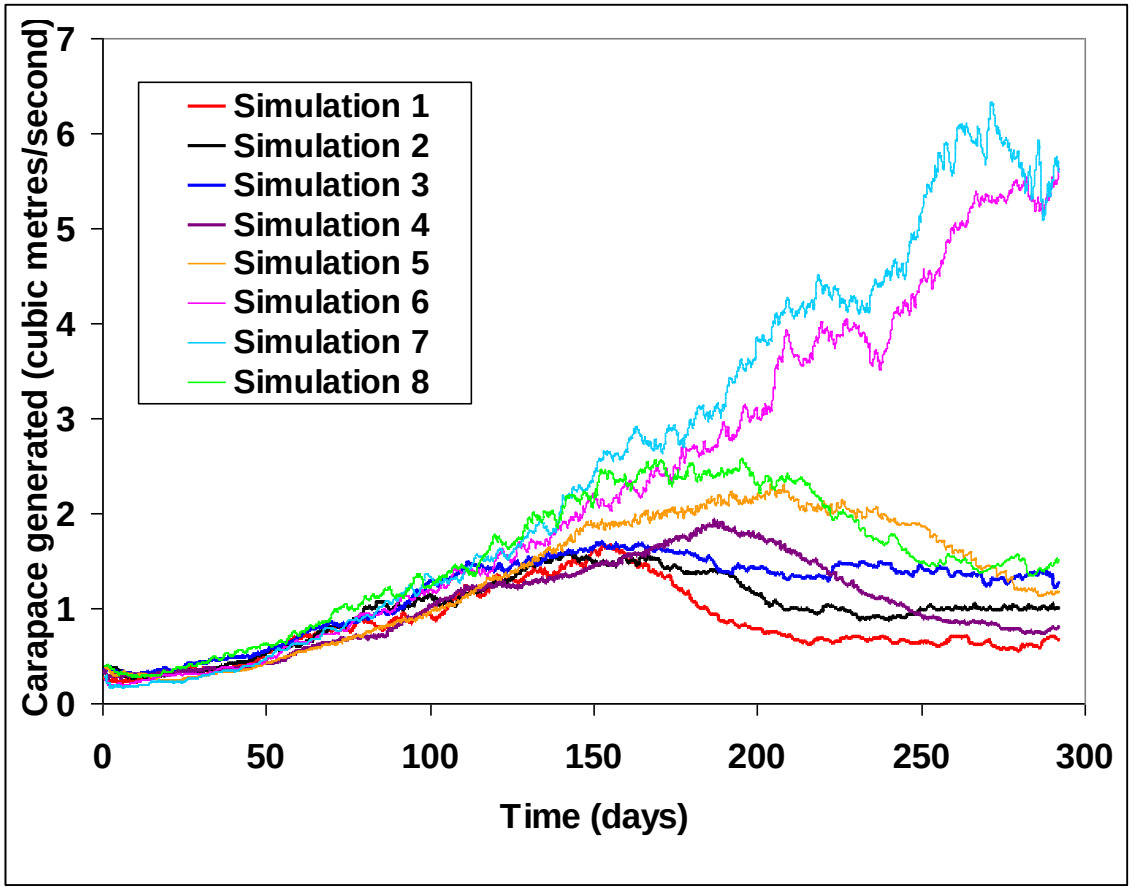

a)

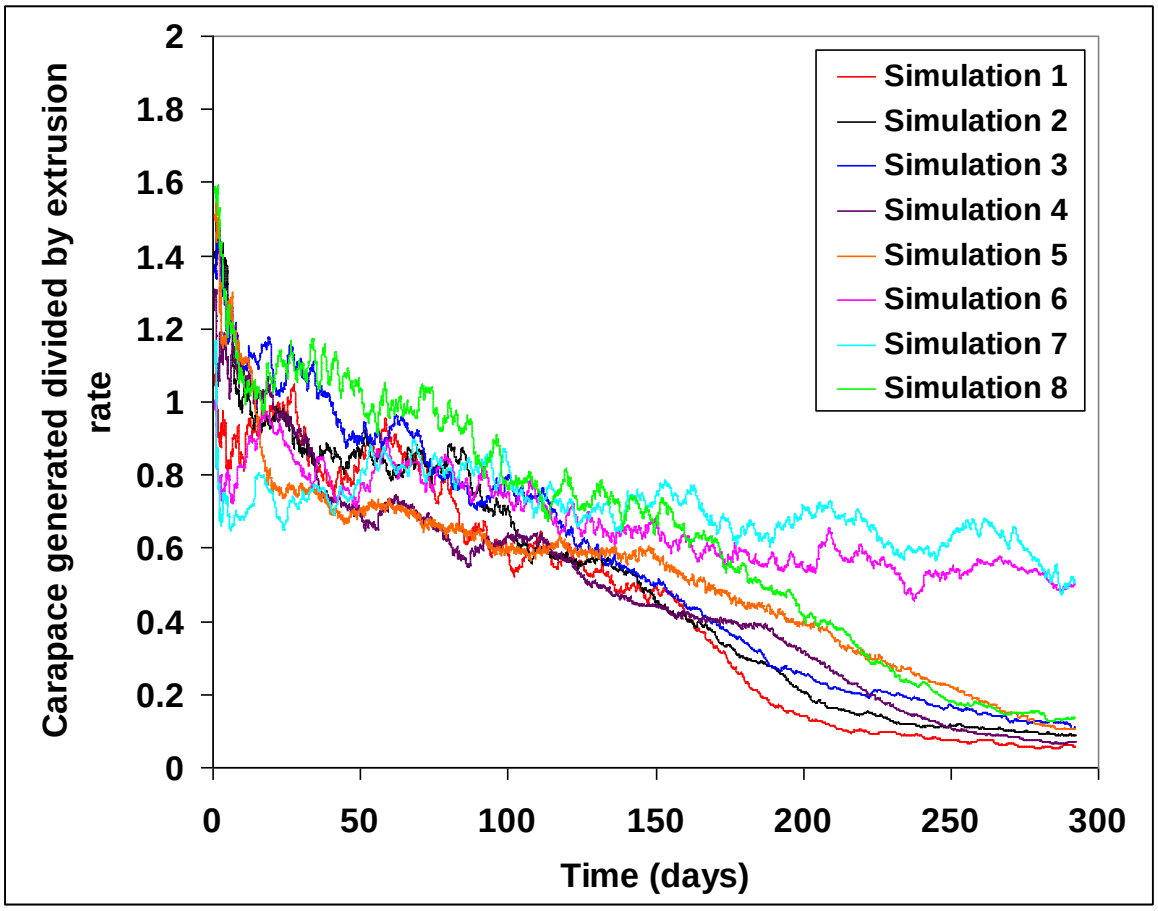

b)

Figure 11 c

Click here to download Figure: Fig11c_Seismic_vs_Aseismic.pdf

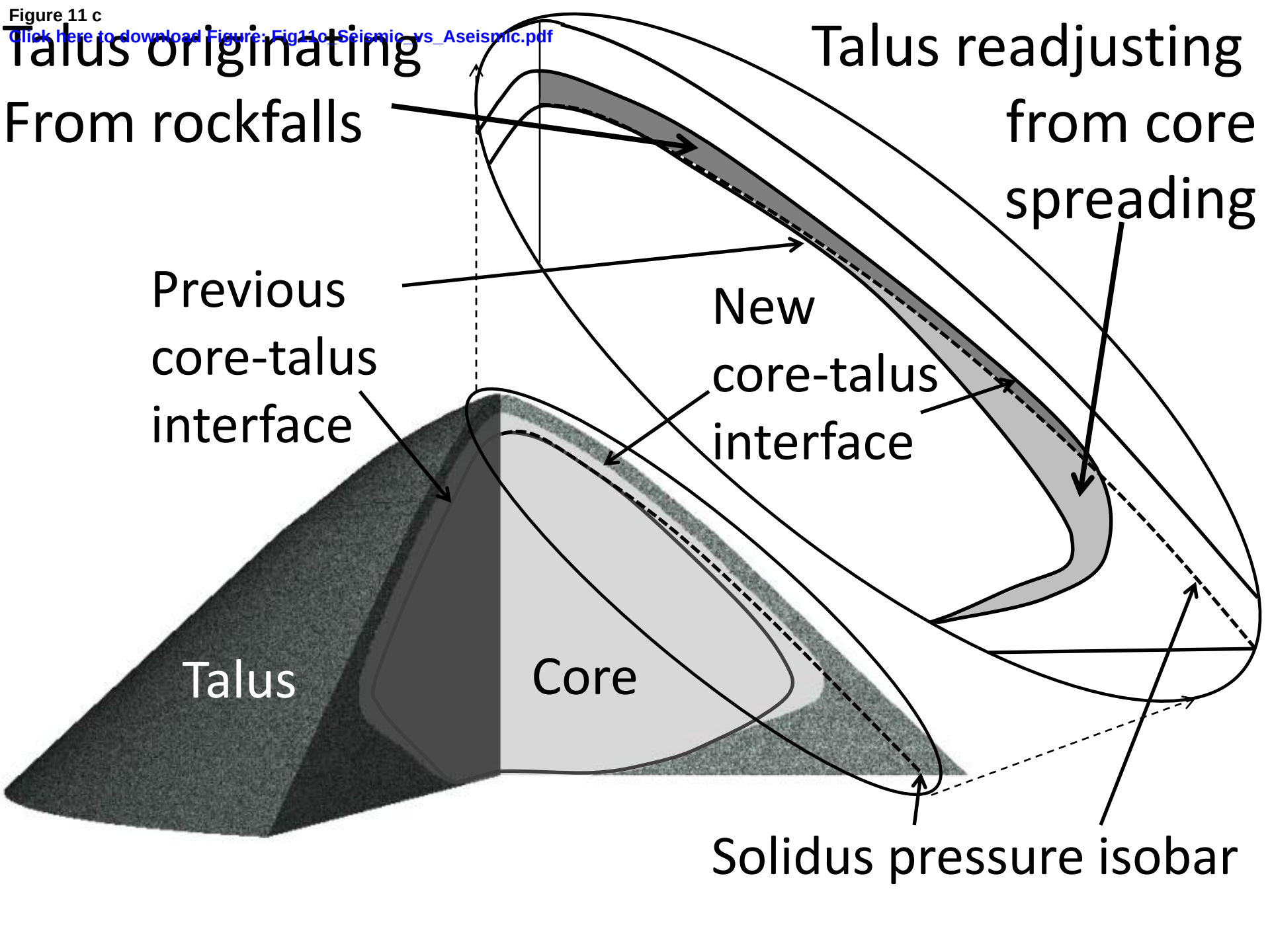

Figure 12
Click here to download Figure: Figures12.pdf

Figure 12:

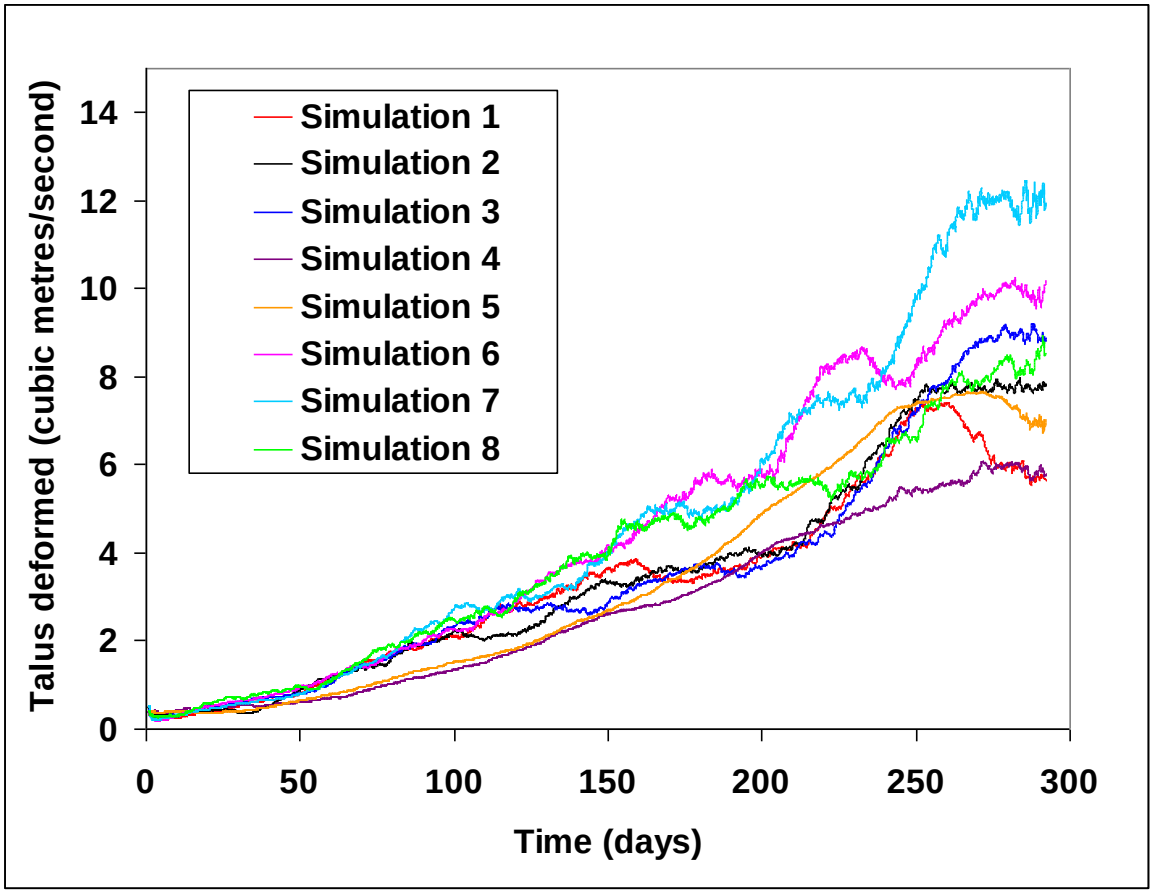

a)

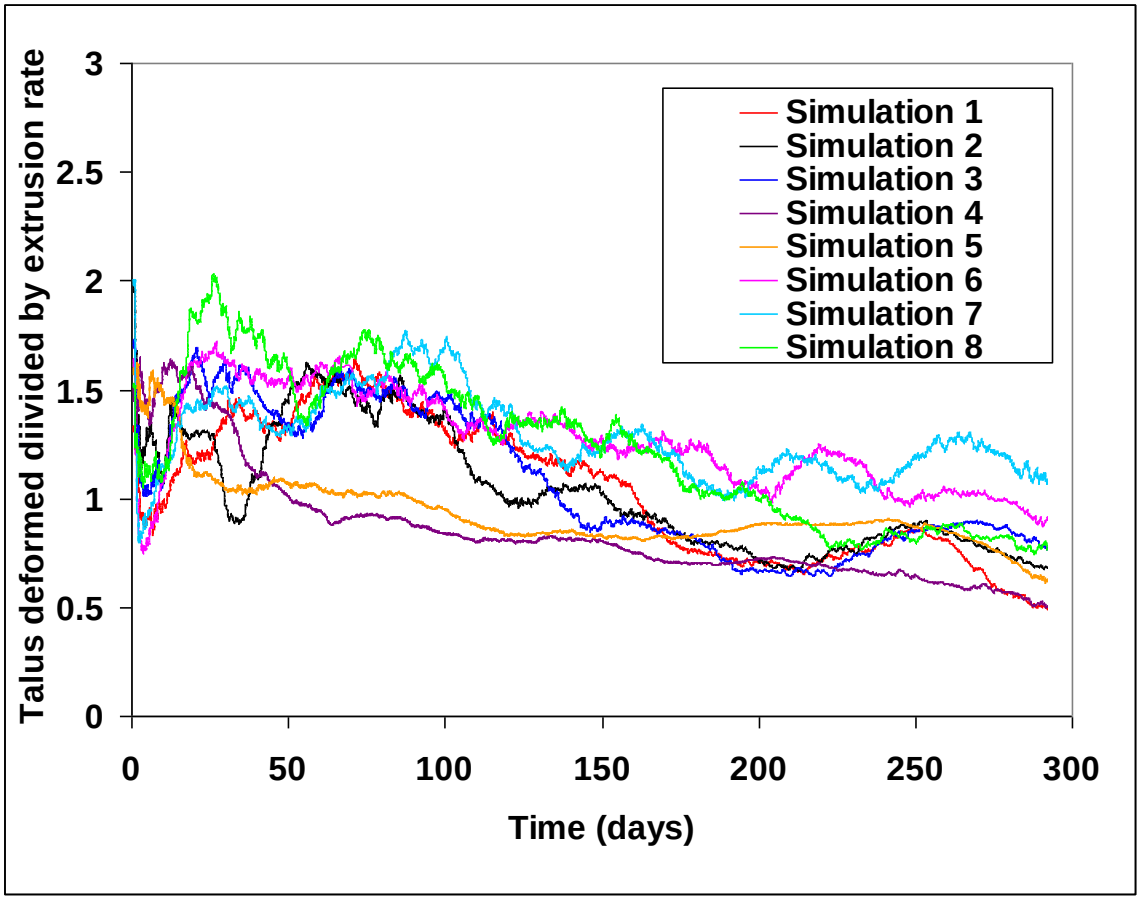

b)

Figure 13

Click here to download high resolution image

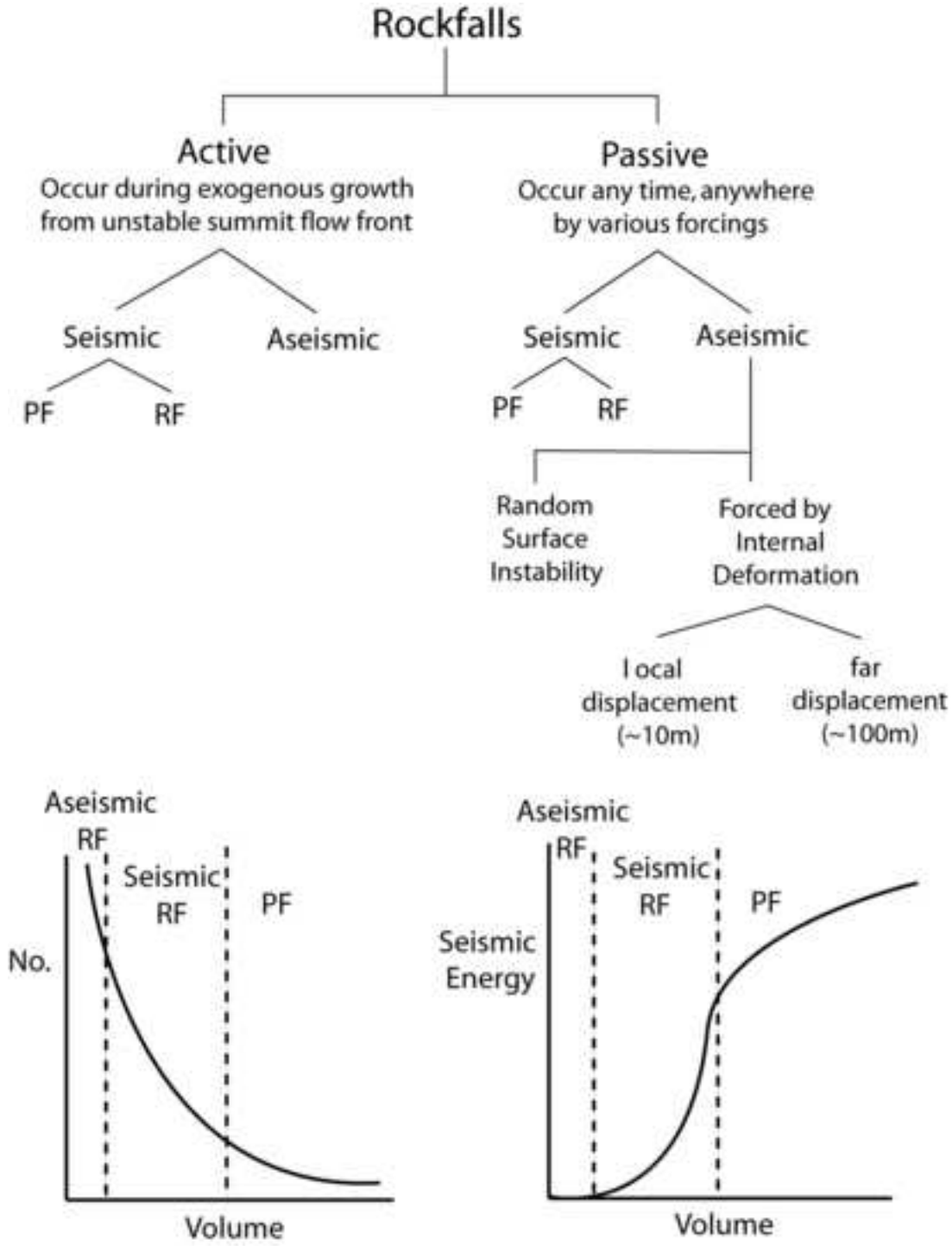

Figure 14
Click here to download Figure: Figures14.pdf

Figure 14:

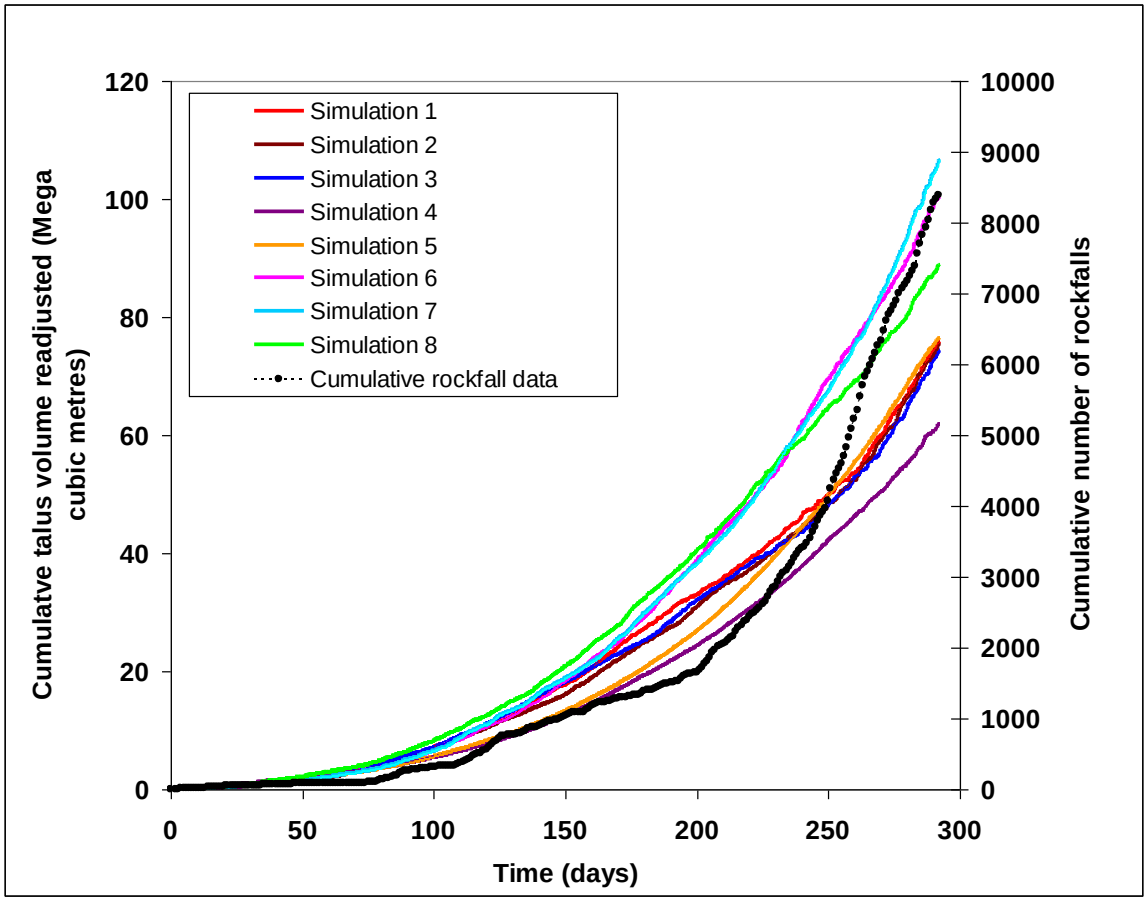

a)

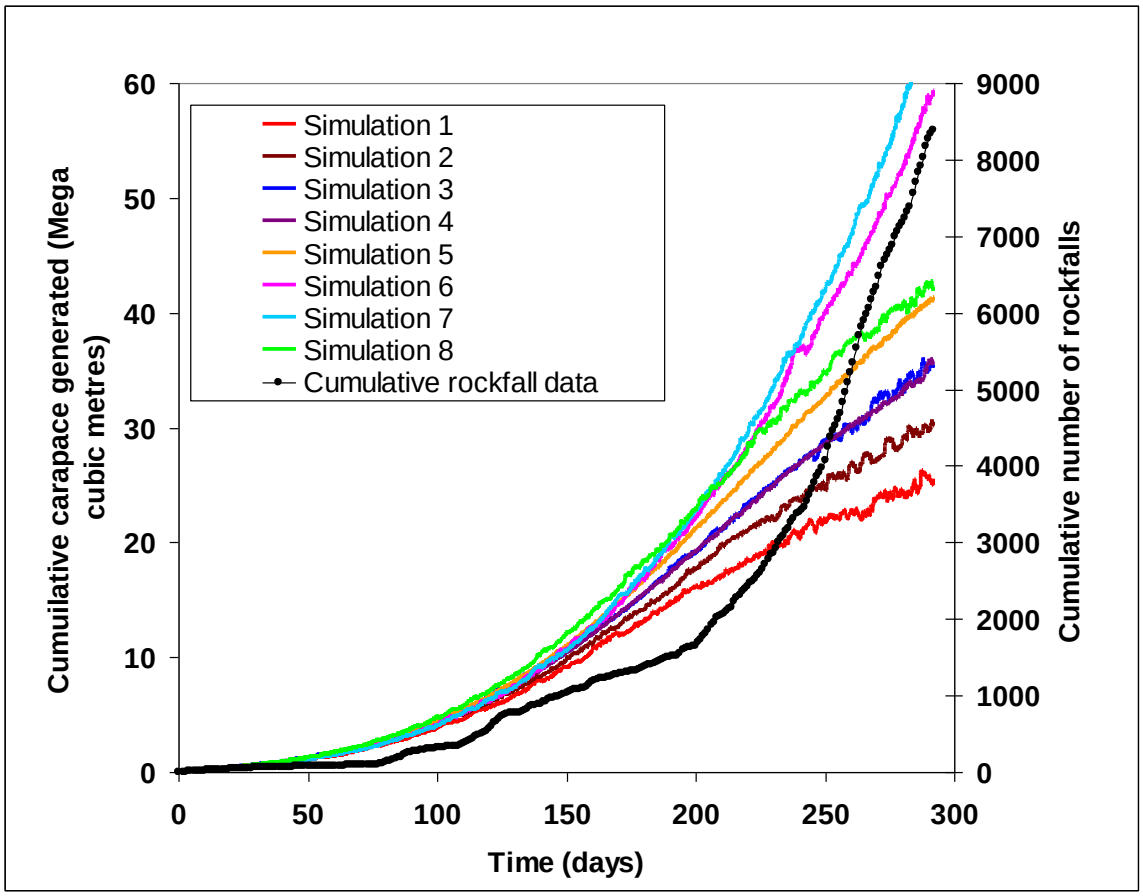

b)

Figure 15

Click here to download Figure: Figures_15.pdf

Figure 15:

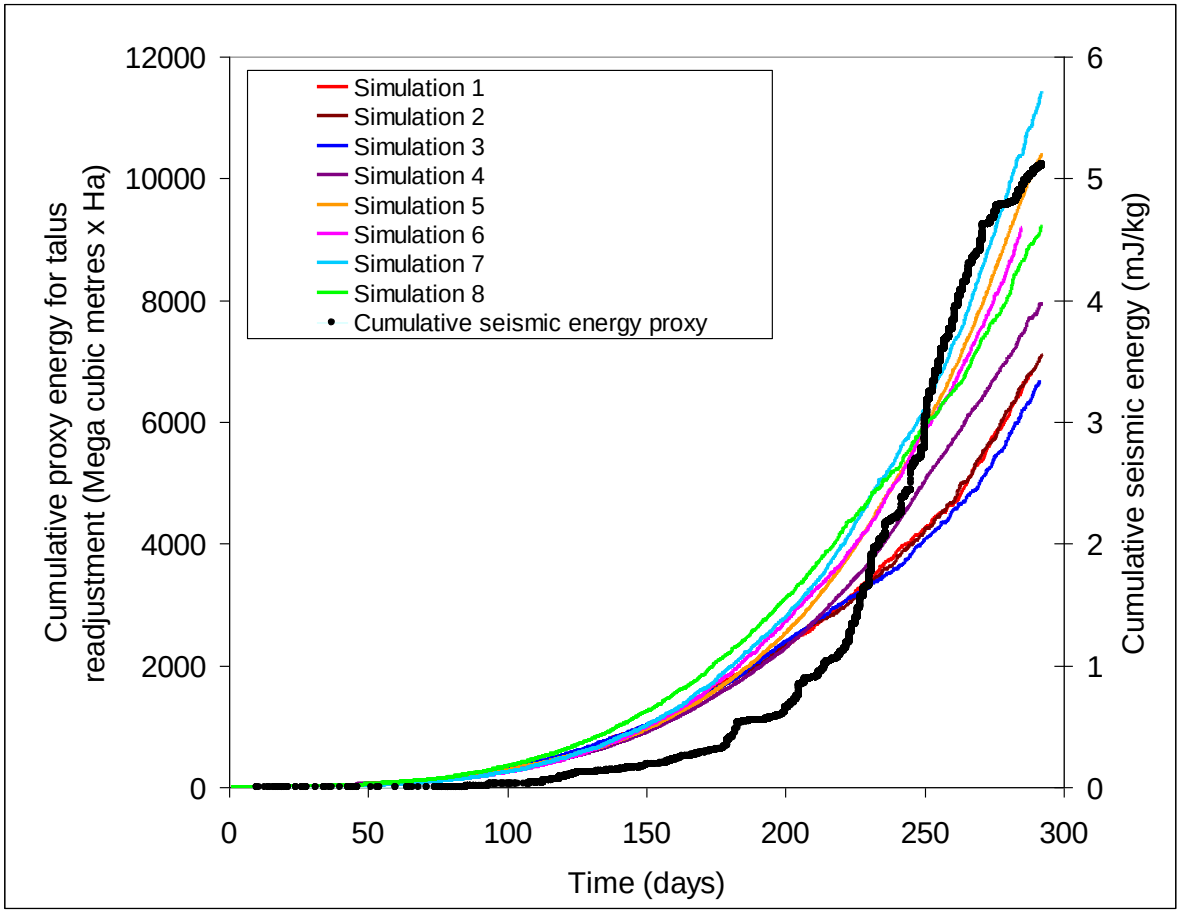

a)

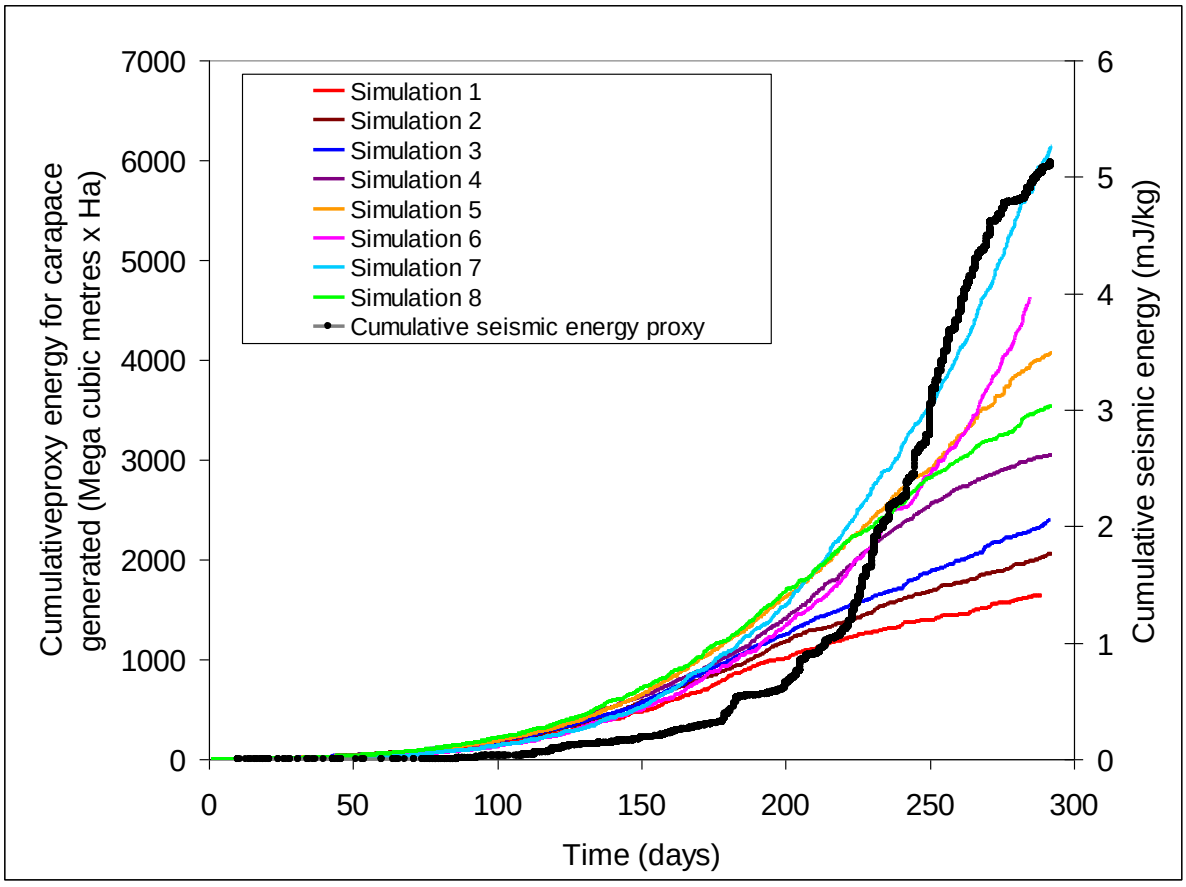

b)